iScience

CellPress

Article

Two New Plasmid Post-segregational Killing Mechanisms for the Implementation of Synthetic Gene Networks in *Escherichia coli*

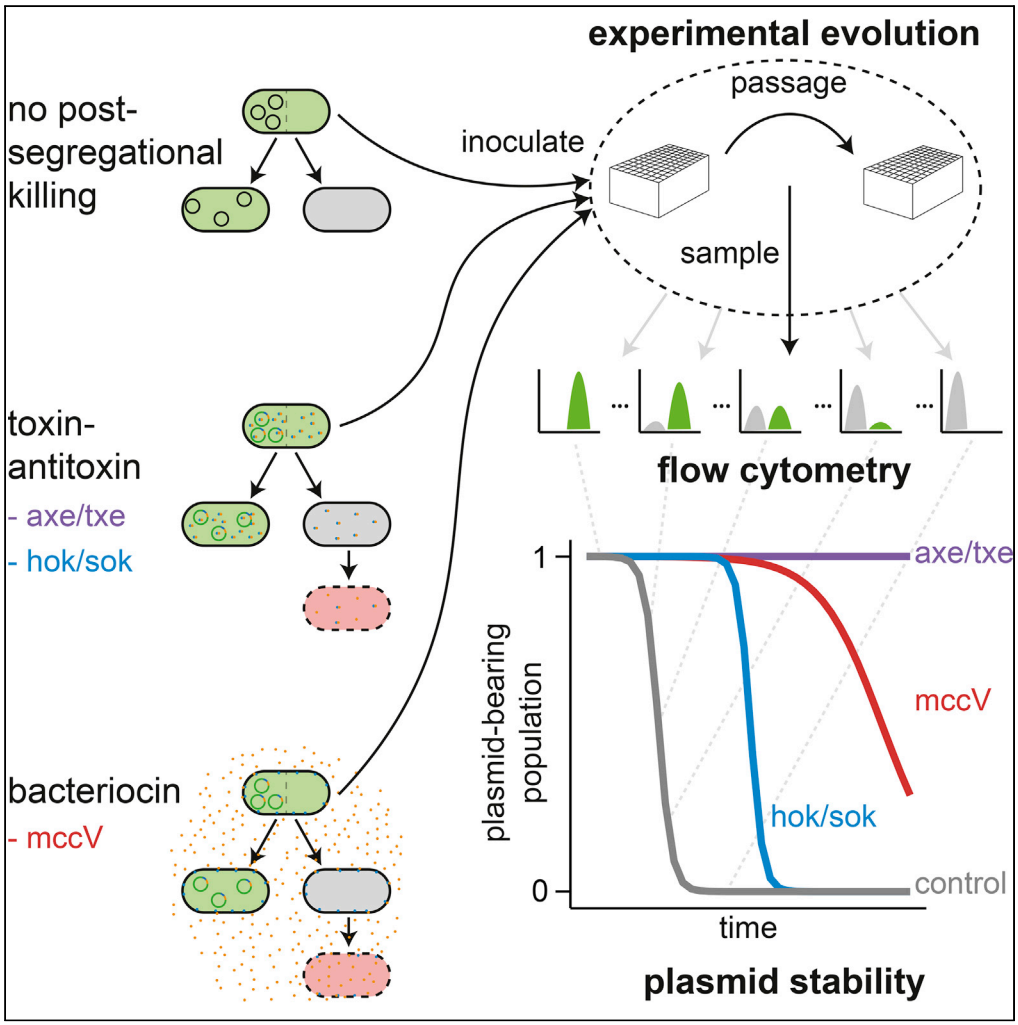

Alex J.H. Fedorec, Tanel Ozdemir, Anjali Doshi, ..., Vitor B. Pinheiro, Tal Danino, Chris P. Barnes

alexander.fedorec.13@ucl.ac.uk (A.J.H.F.)
christopher.barnes@ucl.ac.uk (C.P.B.)

HIGHLIGHTS

axe/txe and microcin-V stabilize plasmids better than hok/sok, the current standard

Microcin-V kills invading plasmid-free cells but is vulnerable to resistant mutants

hok/sok and axe/txe improve plasmid stability in an *in vivo* tumor model

Fedorec et al., iScience *14*, 323–334
April 26, 2019
https://doi.org/10.1016/j.isci.2019.03.019

iScience

CellPress

Article

Two New Plasmid Post-segregational Killing Mechanisms for the Implementation of Synthetic Gene Networks in *Escherichia coli*

Alex J.H. Fedorec,[1,3,9,*] Tanel Ozdemir,[1] Anjali Doshi,[5] Yan-Kay Ho,[4] Luca Rosa,[1] Jack Rutter,[1] Oscar Velazquez,[5] Vitor B. Pinheiro,[4,8] Tal Danino,[5,6,7] and Chris P. Barnes[1,2,9,*]

SUMMARY

Plasmids are the workhorse of both industrial biotechnology and synthetic biology, but ensuring they remain in bacterial cells is a challenge. Antibiotic selection cannot be used to stabilize plasmids in most real-world applications, and inserting dynamical gene networks into the genome remains challenging. Plasmids have evolved several mechanisms for stability, one of which, post-segregational killing (PSK), ensures that plasmid-free cells do not survive. Here we demonstrate the plasmid-stabilizing capabilities of the axe/txe toxin-antitoxin system and the microcin-V bacteriocin system in the probiotic bacteria *Escherichia coli* Nissle 1917 and show that they can outperform the commonly used hok/sok. Using plasmid stability assays, automated flow cytometry analysis, mathematical models, and Bayesian statistics we quantified plasmid stability *in vitro*. Furthermore, we used an *in vivo* mouse cancer model to demonstrate plasmid stability in a real-world therapeutic setting. These new PSK systems, plus the developed Bayesian methodology, will have wide applicability in clinical and industrial biotechnology.

INTRODUCTION

The genes comprising a synthetic circuit can be maintained in a host bacterium in two ways: on the chromosome of the organism or on extra-chromosomal material such as plasmids. Plasmids are a fundamental biological tool and have been widely used in molecular and cellular biology research, leading to a number of well-developed methods for their manipulation (Ellis et al., 2011; Casini et al., 2015). This ease of manipulation enables a level of modularity, which is one of the key engineering goals of synthetic biology (Andrianantoandro et al., 2006; Martinez-Garcia et al., 2014). Plasmid copy number can be an important parameter in the functioning of circuits, and it is non-trivial to convert a dynamical gene circuit from a multi-copy plasmid implementation to a single-copy implementation and maintain identical function (Lee et al., 2016).

However, one of the fundamental problems with using plasmids is their segregational instability. When bacteria divide there is the possibility that all plasmid copies remain in one-half of the cell, which leads to the production of a plasmid-free daughter cell, as shown in Figure 1A. As most of the synthetic circuits that are borne on plasmids produce a burden to their hosts, the plasmid-free population outgrows the plasmid-bearing population and the engineered strain is quickly diluted from the environment (Summers, 1991). Maintaining the presence of the engineered circuit within the bacterial population is fundamentally important in the design of a predictable synthetic biological system.

Antibiotic selection of bacteria-containing plasmids with the corresponding antibiotic resistance genes is commonly used in a research environment. However, antibiotics are not used in industrial fermentation because of the financial impact of removal and deactivation (Kroll et al., 2010). Antibiotics are also unsuitable for clinical applications for a number of reasons including horizontal gene transfer of resistance genes (Stecher et al., 2012; Wright et al., 2008) and the disruption of the native microbiota (Theriot et al., 2014). In light of these limitations, efforts have already been made to reuse a variety of existing microbial mechanisms to ensure plasmid persistence in more complex environments (Kroll et al., 2010; Wright et al., 2013). Successful alternatives have been demonstrated with the use of toxin-antitoxin (TA) systems (Loh and Proft, 2013; Danino et al., 2015), active partitioning mechanisms (Danino et al., 2015; Liu et al., 2005), and auxotrophy (Velur Selvamani et al., 2014a, 2014b).

[1]Department of Cell and Developmental Biology, University College London, London WC1E 6BT, UK

[2]Department of Genetics, Evolution and Environment, University College London, London WC1E 6BT, UK

[3]Centre for Mathematics, Physics and Engineering in the Life Sciences and Experimental Biology, University College London, London WC1E 6BT, UK

[4]Institute of Structural and Molecular Biology, University College London, London WC1E 6BT, UK

[5]Department of Biomedical Engineering, Columbia University, New York City, NY 10027, USA

[6]Data Science Institute, Columbia University, New York, NY 10027, USA

[7]Herbert Irving Comprehensive Cancer Center, Columbia University, New York, NY 10032, USA

[8]KU Leuven Rega Institute for Medical Research, Herestraat, 49 Box 1030, 3000 Leuven, Belgium

[9]Lead Contact

*Correspondence: alexander.fedorec.13@ucl.ac.uk (A.J.H.F.), christopher.barnes@ucl.ac.uk (C.P.B.)

https://doi.org/10.1016/j.isci.2019.03.019

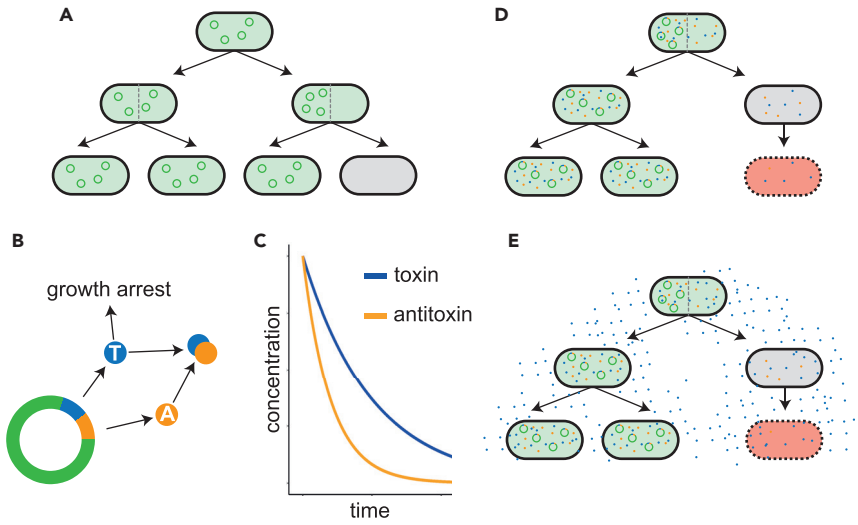

Figure 1. Plasmid Stability and Post-segregational Killing

(A) Plasmid-free cells are produced due to uneven distribution of plasmids at cell division.

(B) Toxin-antitoxin PSK systems are plasmid-borne mechanisms. (C) These systems rely on a long-lived toxin degrading more slowly in a newly plasmid-free cell than the antitoxin.

(D) Post-segregational killing mechanisms carried on plasmids cause the death of cells that lose the plasmid when dividing.

(E) Bacteriocins can improve plasmid stability by a population-level policing through the secretion of a toxin into the environment.

TA systems are a type of post-segregational killing (PSK) mechanism that function through the production of a long-lasting toxin and its shorter-lived antitoxin (Cataudella et al., 2012; Diago-Navarro et al., 2013), both encoded on the plasmid (Figures 1B and 1C). While the plasmid is present in the cell, antitoxin is being produced to neutralize the toxin. If, however, a plasmid-free daughter cell arises, the antitoxin quickly degrades and is unable to be replaced due to lack of the necessary genes. The negative effects of the toxin are no longer prevented, leading to the killing or growth prevention of the cell (Figure 1D). The successful PSK of a plasmid-free cell is reliant on enough toxin becoming active in the cell before it goes on to divide again, further diluting the toxin. Just as with the distribution of plasmids giving a probability of producing plasmid-free cells, there is a probability that the distribution of toxin is such that the TA system fails to kill the newly plasmid-free cell. As such, TA systems are fallible, and once plasmid-free cells escape, they have no mechanism for preventing their growth and the consequent dilution of the plasmid-bearing population. hok/sok is a type I TA system originating from the *parB* locus of the *E. coli* plasmid R1 and has been shown to be effective in its native *E. coli* and the gram-negative *Pseudomonas putida* (Gerdes, 1988). axe/txe is a proteic, type II TA system originating from the axe-txe locus of the gram-positive *Enterococcus faecium* plasmid pRUM (Grady and Hayes, 2003). It has been demonstrated that axe/txe could be used to stabilize a luminescent reporter in the gram-positive *Enterococcus faecalis in vivo* without antibiotic selection for 5 days (Rosa et al., 2013). The axe/txe system was also found to be present in 75% of vancomycin-resistant enterococci isolates, a common hospital pathogen and growing global concern (Moritz and Hergenrother, 2007).

An alternative to TA systems are bacteriocins, which are bacterially secreted proteins that have a bactericidal effect on either a narrow or broad spectrum of other bacteria lacking immunity (Riley, 1998). By secreting these antimicrobial peptides, a plasmid-bearing population is able to police the environment, preventing the growth of plasmid-free cells (depicted in Figure 1E). Successful attempts have already been made to use bacteriocins, such as the Lcn972 system, to stabilize plasmids in *Lactococcus lactis* (Campelo et al., 2014) and the colicins A and E2 in *E. coli* (Inglis et al., 2013). Here we use the microcin-V system, which is encoded on conjugative plasmids in *E. coli*. It consists of a low-molecular-weight toxic bacteriocin, which kills through pore formation, along with the genes for an ABC transporter and immunity protein (Azpiroz and Laviña, 2007). Microcin-V does not undergo any post-translational modification and, as such, does not require any additional enzyme-encoding genes. The structure of the bacteriocin gene

itself is also modular, which allows for its hybridization with other bacteriocins, enabling the targeting of other bacterial strains (Acuña et al., 2012, 2015). Furthermore, it has been shown that *E. coli* Nissle (EcN) already carries two bacteriocin systems in its chromosome, microcins H47 and M (Grozdanov et al., 2004). More recently, it was also shown that native bacteriocins found in EcN were vital in mediating competition in the inflamed gut in an inter- and intraspecies manner (Sassone-Corsi et al., 2016).

In this work we develop a mathematical model that describes how PSK systems improve plasmid maintenance. Using several origins of replication, we show how plasmid copy number and burden affect plasmid stability, with and without a TA system. We use our mathematical model and develop a Bayesian inference procedure to quantify the efficacy of two PSK systems, axe/txe and microcin-V, in stabilizing a burdensome plasmid in EcN and compare them to the more commonly used hok/sok system. The model enables determination of PSK efficacy and also the extra metabolic burden due to the PSK system. We show that the bacteriocin, unlike the TA systems, is able to remove plasmid-free bacteria from an environment if they arise. We also investigate the ability of the PSK systems in stabilizing a luminescent reporter plasmid without antibiotic selection *in vitro* and in a mouse tumor xenograft model *in vivo*. Collectively, we show that the two new systems show a much greater potential for plasmid stabilization than hok/sok in EcN.

RESULTS

A Mathematical Model for Plasmid Loss and Post-segregational Killing

Early mathematical models of plasmid stability consisted of terms for a plasmid-bearing population and plasmid-free population, growing exponentially at different rates with a constant probability of plasmid loss from the plasmid-bearing population (Boe et al., 1987). These models were used to determine plasmid loss rates from experimental data (Boe, 1996; Boe and Rasmussen, 1996) and extended to describe bacterial populations in a chemostat, introducing dilution as well as growth rates dependent on a substrate (Ganusov and Brilkov, 2002). A more detailed model of plasmid loss was devised that takes into account the age distribution of bacteria within a population, although the predictions produced were virtually indistinguishable from simpler models (Lau et al., 2013). However, this model did highlight the difficulties of trying to infer the plasmid loss rate from measured population data as, due to the exceedingly small plasmid loss rates of most systems, the growth rate differences dominate the dynamics and lead to overestimation of plasmid loss (Lau et al., 2013).

Here, we extend the early plasmid loss model (Boe, 1996) to include PSK by a TA system. In this model there are two populations, plasmid-bearing (X^+) and plasmid-free (X^-) populations

$$\frac{dX^+}{d\tau} = \gamma X^+ - \lambda\gamma X^+$$
$$\frac{dX^-}{d\tau} = X^- + \lambda\gamma X^+ - \omega\lambda\gamma X^+ \qquad \text{(Equation 1)}$$

where λ is the probability of producing a plasmid-free daughter cell when a plasmid-bearing cell divides, γ is the ratio of plasmid-free doubling time to plasmid-bearing doubling time, and ω is the probability of successful PSK. The time step, τ, is equal to one plasmid-free generation.

Bacteriocins do not produce PSK in the traditional sense. Instead there is a constant killing pressure on the plasmid-free population rather than specific killing of newly plasmid free cells. As such, the equation for the change in plasmid-free population differs to take into account the different point at which the bacteriocin causes the death of plasmid-free cells.

$$\frac{dX^-}{d\tau} = X^- + \lambda\gamma X^+ - 2\omega X^- \qquad \text{(Equation 2)}$$

Figure S1 shows the effects of varying each of the model parameters on the dynamics of plasmid loss. The plasmid loss parameter, λ, which is related to average plasmid copy number, n, according to $\lambda = 2^{1-n}$ (Summers, 1991), affects the gradient of the plasmid loss curves early on, when there are very few plasmid-free cells. As soon as a plasmid-free population is established, the doubling time ratio, γ, which is a measure of the burden placed on the cell by the plasmid, has a large effect on the gradient. For the TA model in Equation 1, the killing parameter, ω, has a similar effect on the parameter λ. This is because it acts to delay the establishment of a plasmid-free population. The killing parameter in the bacteriocin model produces different dynamics to that for the TA model as it acts on all plasmid-free cells rather

than just newly plasmid-free cells. A hierarchical Bayesian method for fitting the model to data allows these parameters to be determined from simulated and experimental plasmid loss curves (Transparent Methods, Figure S2).

Plasmid Copy Number and Burden Affect Plasmid Stability

A series of fluorescent reporter plasmids, expressing dasher GFP from the strong constitutive OXB20 promoter, were produced with four different origins of replication (Figure 2A), which would offer a range of plasmid copy numbers (Jahn et al., 2016). The SC101 origin, without native active partitioning system, provided a low plasmid copy number; p15A, a medium copy number; ColE1, a high copy number; and pUC, a very high copy number. Quantitative PCR (qPCR) was carried out to determine the copy number of these plasmids within EcN-Lux. Primers for plasmid amplification were chosen within the kanamycin resistance gene. This region is common across all the plasmids we used, negating the need to design primers for each plasmid. The qPCR results (Figure 2B) show that the SC101 origin does, indeed, produce the lowest plasmid copy number (~4.8). The p15A origin has a slightly higher copy number (~12), and the hybrid ColE1-RO1600 origin has an even higher copy number (~21). However, the pUC origin is far from the very high copy number that has been reported in the literature previously (Yanisch-Perron et al., 1985) and is comparable with the p15A origin (~14.5). Furthermore, the variance in copy number for the hybrid ColE1-RO1600 is large, with the highest copy replicate roughly four times higher than the median. These plasmid copy numbers are broadly in agreement with other recent estimates (Jahn et al., 2016).

Using a microplate reader to collect growth data and a non-parametric Gaussian process method to fit the growth curves (Swain et al., 2016), we were able to quantify the effect of carrying plasmids with different replication origins. The growth curves and model fits from which the maximal growth rates are estimated are shown in Figure S3. Growth rate measurements for each of the plasmids in EcN-Lux mirror the plasmid copy numbers measured using qPCR; the low copy SC101 plasmid has the lowest impact on growth rate, whereas the highest copy ColE1-RO1600 origin produces the greatest burden (Figure 2C). These results demonstrate the problem for plasmid stability; once the plasmid is dropped, the significantly higher growth in the plasmid-free strain causes the plasmid-bearing population to be outcompeted.

A daily passaging method was used to gather flow cytometry data, which was analyzed using an automated analysis pipeline (Transparent Methods, Figures S4–S11). This allowed us to determine plasmid stability over 21 days for the strains bearing plasmids with each of the four different replication origins, with and without the hok/sok TA system (Figure 2D). Our results are contrary to the conventional wisdom that a lower copy number plasmid will be lost sooner. Here we show that, in fact, the higher copy number plasmids, ColE1-RO1600 and pUC are lost sooner than the lowest copy SC101-based plasmid. This pattern is also reflected when the plasmids carry the hok/sok TA system. However, the p15A-based plasmid with the hok/sok system performs best, suggesting that there may be an optimum plasmid copy number for such TA systems.

Toxin-Antitoxin Systems Minimally Impact Growth Rates

The pUC-based fluorescence reporter plasmid was used to determine the efficacy of three different plasmid-stability mechanisms: hok/sok, axe/txe, and microcin-V (Figure 3A). This plasmid was chosen as, from the above results, it resulted in the fastest plasmid loss of the four replication origins tested. qPCR was again used to determine the effect on plasmid copy number of carrying the different plasmid stability mechanisms (Figure 3B). This showed no difference between the control plasmid and the hok/sok-carrying plasmid. However, the axe/txe system shows a slight, but insignificant, increase in copy number, whereas the bacteriocin system shows a slight decrease in copy number.

Growth rates were assayed, and the maximal growth rates were determined (Figure 3C). The growth curves and model fits from which the maximum growth rates are estimated are shown in Figure S12. The maximal growth rates show a significant load on the growth rate between plasmid-free EcN-Lux and the plasmid-bearing strains. The TA systems have similar growth rates to the pUC-GFP control plasmid, repeating the pattern of plasmid copy number as an indicator of growth rate. However, the bacteriocin system, even with the slightly lower copy number measured from qPCR, has a slower growth rate than the other plasmids.

Both axe/txe and Microcin-V Outperform hok/sok in Liquid Culture

Flow cytometry data (Figures S13–S16) were gathered using our daily passaging method and were used to derive plasmid loss curves for the pUC-GFP-based fluorescent plasmids in EcN-Lux over 37 daily passages

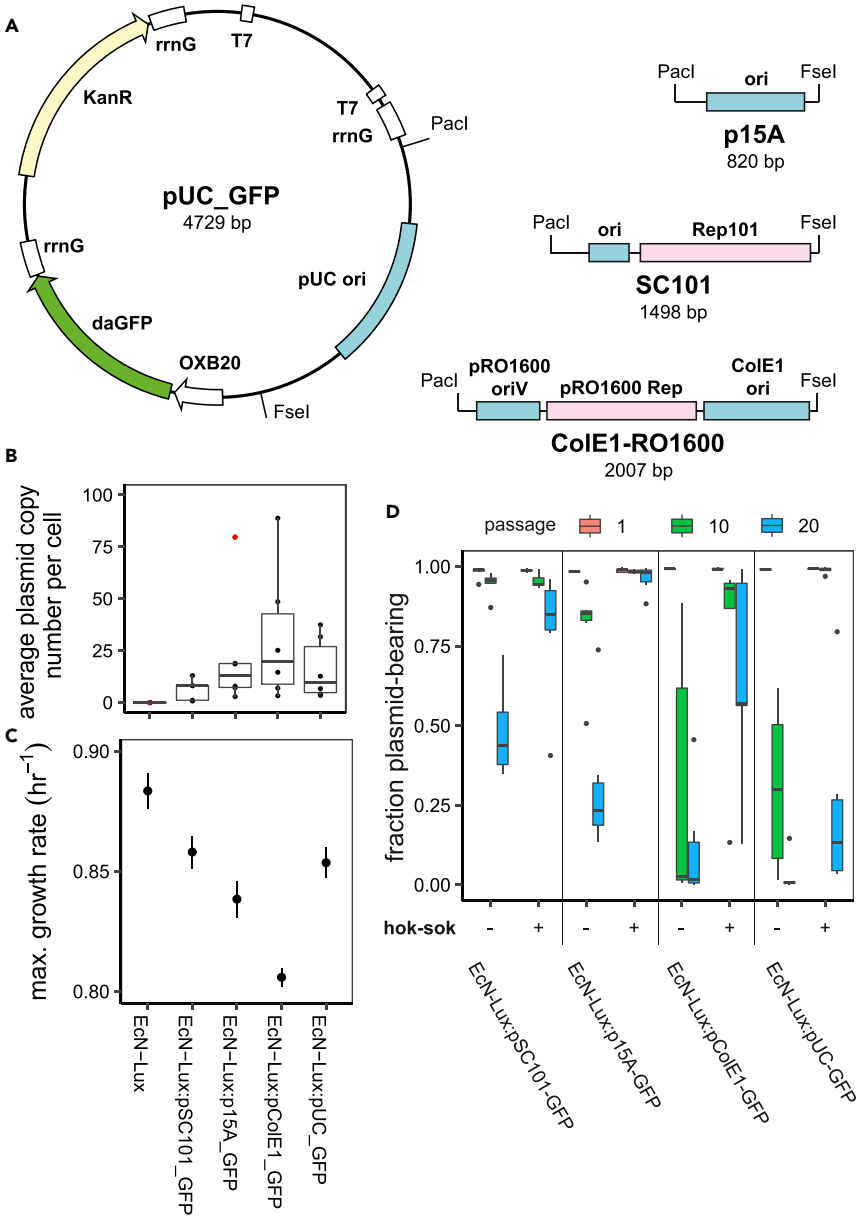

Figure 2. Plasmid Origin of Replication Affects Segregational Stability

(A) Plasmids with different origins of replication were produced, constitutively expressing GFP.

(B) Using qPCR, average plasmid copy number was calculated for each of the origins of replication. (Circles show samples, red circles are considered outliers.)

(C) Changes in bacterial growth rate correspond to differences in plasmid copy number, with the higher-copy plasmids producing a larger reduction in maximal growth rate. (Filled circles show the mean calculated maximal growth rates, and lines show standard deviations.)

(D) The effects of plasmid copy number and growth rate, dictated by the origin of replication, combine to alter the segregational stability of the different plasmids over 3 weeks of passaging. Although the commonly used hok/sok toxin-antitoxin system is able to increase stability, none of the plasmids are perfectly maintained over 20 days. (Black circles show outliers.)

(Figure 3D). For the control plasmid, without a PSK system (EcN-Lux:pUCGFP), the plasmid-free cells start to become apparent after only ~4 passages, with the populations becoming entirely plasmid free after ~12 passages. Figures 3D and S17 show that the TA systems improve the stability of the plasmid, although the commonly used hok/sok (EcN-Lux:pUC-GFP-HS) only provides stability for ~16 passages, with one

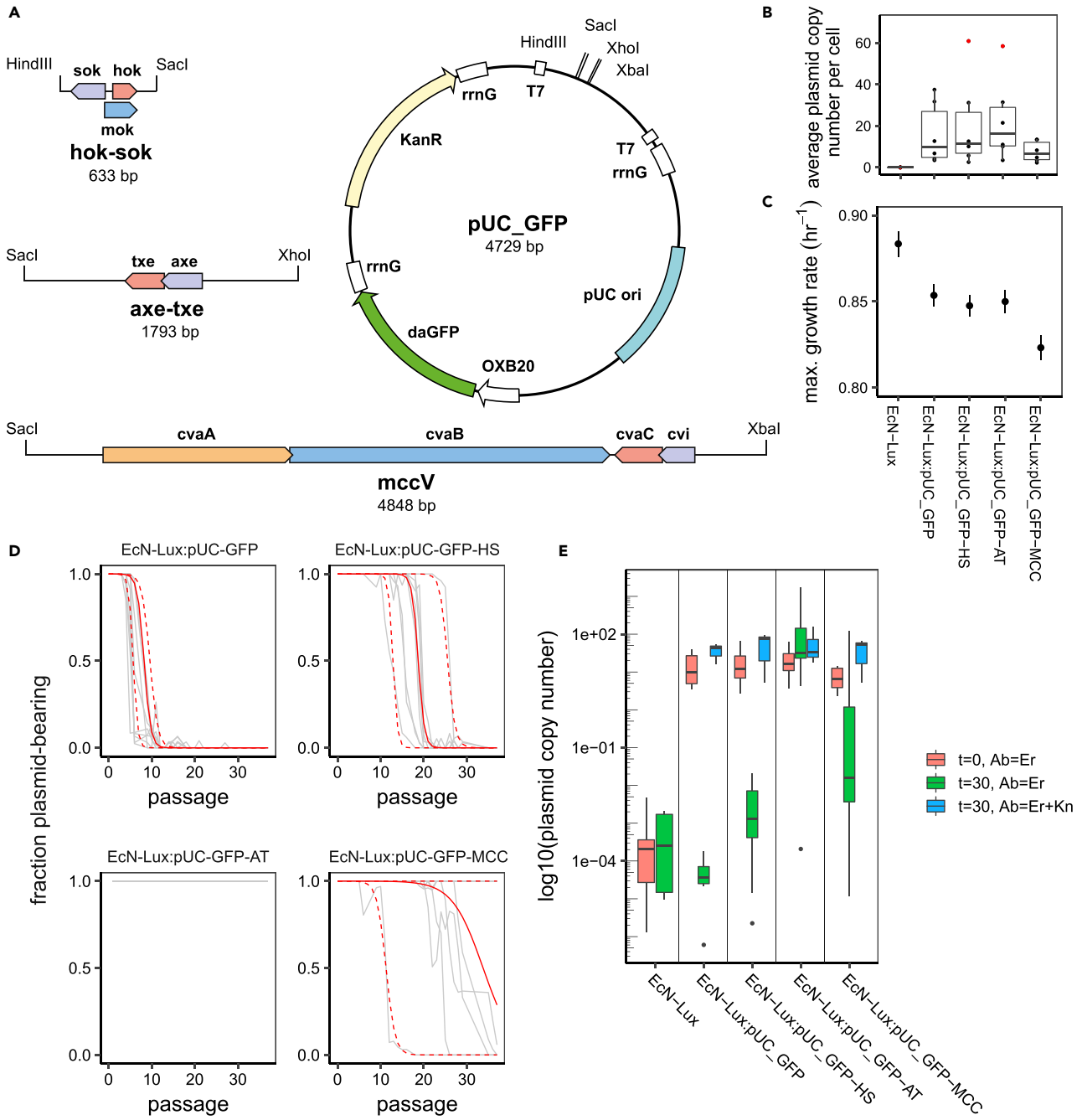

Figure 3. Plasmid Stability Mechanisms Have Varying Efficacy

(A) Two toxin-antitoxin and one bacteriocin mechanism were cloned into the pUC-based burdensome plasmid and transformed into EcN-Lux.

(B) qPCR shows that the two toxin-antitoxin systems have minimal effect on plasmid copy number. The bacteriocin system, however, seems to reduce copy number slightly. (Circles show samples, red circles are considered outliers.)

(C) Maximal growth rates show that the burden of carrying the toxin-antitoxin systems does not affect growth. However, even with a lower copy number, the bacteriocin system shows a reduced maximal growth rate. (Filled circles show the mean calculated maximal growth rates, and lines show standard deviations.)

(D) Plasmid loss curves for fluorescence-based plasmids in EcN-Lux. The gray lines show the trajectories of nine replicates for each strain. The solid red line shows the average model fit, and the dashed red lines show the 95% confidence intervals of the model with posteriors from all replicates.

(E) qPCR carried out before undergoing passaging, after 30 days of passaging, and after 30 days of passaging with plasmid maintenance enforced by antibiotic selection. These back up the plasmid loss seen in the curves calculated from flow cytometry data (D). (Black circles show outliers.)

replicate beginning to drop as soon as passage 10 and one lasting until passage 22. Fitting our model to the data shows that the hok/sok system has a very high killing efficacy, with a survival probability of less than 5×10^{-5} (Figure S18) but still loses out to competition from the few plasmid-free cells that escape the toxin. Strikingly, axe/txe (EcN-Lux:pUC-GFP-AT) remains stable throughout the experiment, clearly demonstrating its efficacy over the other systems. As no plasmid loss is observed, the model-fitting procedure cannot be applied as there is no information on the probability of plasmid loss, λ. Finally, the results demonstrate that the microcin-V system (EcN-Lux:pUC-GFPMCC) outperforms the hok/sok system, although the results are varied, with four of the nine replicates remaining entirely plasmid bearing for the length of the experiment and in five of the replicates we see a plasmid-free population taking over. The model determined that efficiency of the bacteriocin killing is far below that of hok/sok, although, due to its population-scale effect, it still manages to produce stable populations for a longer period (Figure S18).

qPCR was carried out to determine how the plasmid copy number had changed, from the initial cultures to the cultures after 30 passages, in both the selective (erythromycin and kanamycin) and non-selective (only erythromycin) conditions (Figure 3E). After 30 passages of growth under selective conditions, the plasmid copy number had slightly increased for all the plasmids. This may be due to the enforced co-existence of the plasmids in the host leading to compensatory changes within the host or plasmid (Bouma and Lenski, 1988). The raw flow cytometry data show that when plasmid maintenance is enforced through the use of antibiotics the fluorescence levels remain stable across the full 37 passages for all but the microcin-V-bearing strain (Figures S13–S16). For the control plasmid and two TA system plasmids, this suggests that there is compensation between gene expression and copy number, which leads to the overall maintenance of fluorescence level. This conclusion is further supported by the population-level fluorescence data recorded using a microplate reader (Figure S17).

The average plasmid copy number after 30 passages of growth under non-selective conditions reinforces the results determined using flow cytometry. The control plasmid (EcN-Lux:pUC-GFP) has been completely lost, with levels comparable to the EcN-Lux strain with no plasmid. The hok/sok-carrying plasmid (EcN-Lux:pUC-GFP-HS) is similarly low, although there may be a small number of plasmids still present within the population that have not been removed through passaging. As was seen with the flow cytometry data, the axe/txe-bearing plasmid is still entirely present, and at levels comparable to the strains grown in selective media. Finally, the broad spread of copy numbers seen in the microcin-V system (EcN-Lux:pUC-GFP-MCC) reflects the heterogeneity seen in the flow cytometry data. Some of the replicates have completely lost the plasmid, whereas others are at an intermediate stage or are still plasmid bearing.

Microcin-V Can Restore a Plasmid-Bearing Population

As we have seen with hok/sok, once plasmid-free cells arise in the population the TA system has no way to save the plasmid-bearing population. Bacteriocins, however, are able to police the entire population due to the toxin being secreted into the environment. This means that when plasmid-free cells arise or if the culture becomes contaminated, the bacteriocin system can push the population back toward entirely plasmid bearing.

Figure 4 shows that when a population of TA plasmid-bearing cells is diluted with plasmid-free EcN-Lux, the plasmid-free population outgrows the plasmid-bearing population, further diluting it. However, when we dilute the EcN-Lux:pUC-GFP-MCC cells, they quickly kill the plasmid-free population and restore the population. In fact, within 24 h there are no plasmid-free cells detectable in all but one anomalous sample.

Microcin-V Instability Is Due to Immunity Development

As we have shown that the bacteriocin has the ability to kill plasmid-free cells introduced to their environment (Figure 4), why is there plasmid loss in Figure 3D? Three possibilities are the entire population is still plasmid bearing but some are no longer GFP expressing, the plasmid-bearing cells are no longer expressing the bacteriocin, or plasmid-free cells have developed immunity. To test these possibilities we used the cultures from the 30th passage of the plasmid loss experiment. These cultures were grown for 6 h with and without kanamycin selection. The cultures grown non-selectively reflect the state of the population at the time of being passaged. They were spotted next to a bacteriocin-producing, EcN-Lux:pUC-GFP-MCC,

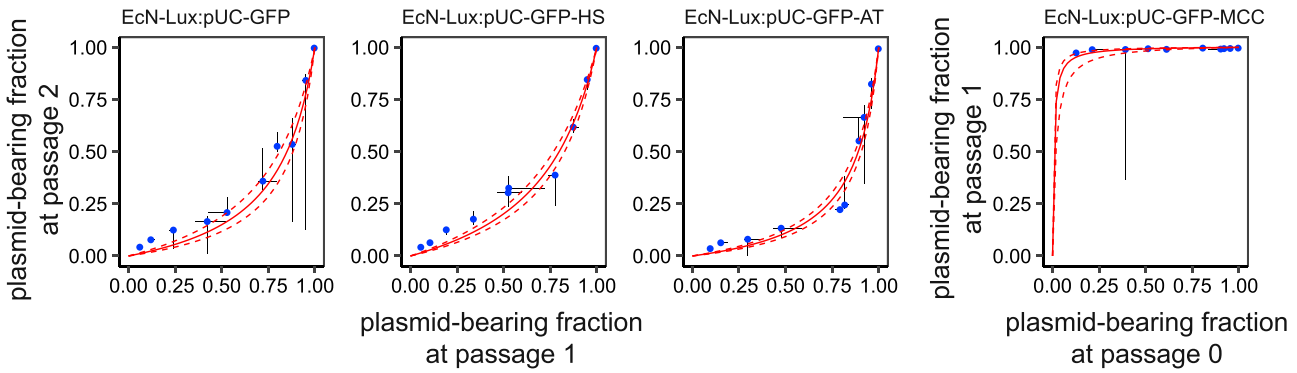

Figure 4. Plasmid-Bearing Strains Are Diluted with Plasmid-Free EcN-Lux at Different Ratios

The dilutions are sampled after 24 h and show that the faster growth rate of the plasmid-free cells leads to further dilution of the plasmid-bearing population. In the case of EcN-Lux:pUC-GFP-MCC, however, the secreted bacteriocin allows the plasmid-bearing population to outcompete the plasmid-free cells. Blue points show the median of three replicates at each initial dilution; the bars show the minimum and maximum plasmid-bearing fraction at each passage. The solid red line shows the model fit, and the dashed red lines show the 95% confidence intervals. Each replicate was passaged once initially to allow for the cells to acclimatize to the growth conditions. However, for the EcN-Lux:pUC-GFP-MCC replicates, most plasmid-free cells were dead after one passage so the data from passage 0 to passage 1 were used.

colony to determine if there was bacteriocin immunity in the population (Figure S19). All the colonies grew, indicating the presence of immune cells. Furthermore, fluorescence levels were not at the level of the colonies grown under kanamycin selection, indicating that it is not just plasmid-bearing cells surviving the bacteriocin. The cultures grown selectively were spotted next to bacteriocin-sensitive EcN-Lux colonies. The first point to note is that two of the colonies grew very little, suggesting almost complete loss of any residual plasmid-bearing cells from those cultures. Furthermore, the fluorescence levels of all the other colonies are greater than those of the colonies grown non-selectively. This indicates that plasmid-bearing cells, expressing GFP, are still present in these cultures but are diluted by kanamycin-sensitive, plasmid-free bacteria. Finally, for all but one of the colonies that grew under selective conditions, the growth of the bacteriocin-sensitive strain spotted next to them is inhibited. This shows that there are still bacteriocin-producing cells within those colonies. These observations together show that the plasmid loss seen in Figure 3D for the pUC-GFP-MCC-bearing strain is due to the development of immunity by plasmid-free bacteria (Feldgarden and Riley, 1999), not the loss of the ability to produce bacteriocin.

axe/txe and hok/sok Successfully Stabilizes Luminescent Reporters *In Vivo*

We produced a luminescent reporter plasmid, p24-Lux, that constitutively expresses the *luxCDABE* operon from the phelp promoter (Riedel et al., 2007) and cloned in the three PSK systems, so that we could visualize its presence *in vivo* (Figure 5A). Plasmid stability for these luminescent plasmids was then determined using the same protocol as for the fluorescent pUC-GFP-based strains. However, measurements could only be carried out using population luminescence in a microplate reader rather than single-cell fluorescence in a flow cytometer. Figure S20 shows that the control population (EcN:p24-Lux) has almost completely stopped luminescing by the end of the first passage. The two TA strains and the microcin-V-carrying strain perform better than the control and rank in the same order as the fluorescent plasmids. However, the luminescence loss occurs faster and even affects the axe/txe-bearing strain.

EcN strains containing the p24-Lux-HS, p24-Lux-AT, p24-Lux-MCC, or p24-Lux control constructs were intravenously injected into a mouse tumor model for *in vivo* characterization (Danino et al., 2015). Once administered, the EcN strain was shown to colonize the tumors in the mouse flanks within 3 days (Figure 5A). The mice were visualized daily, and luminescence readings were taken to determine the presence of protein production by our engineered bacteria within each tumor. Regions of interest (ROIs) were manually drawn around each tumor. The average radiance across each ROI (Figure 5C) shows the colonization and continued production of luminescence by the strains. The luminescence peaks between 3 and 4 days after administration and then begins to decline. However, the luminescence of tumors for mice administered with the EcN-Lux strain without plasmid, continues to increase, indicating that the continued presence of bacteria in the tumors is possible. This indicates that the decline in

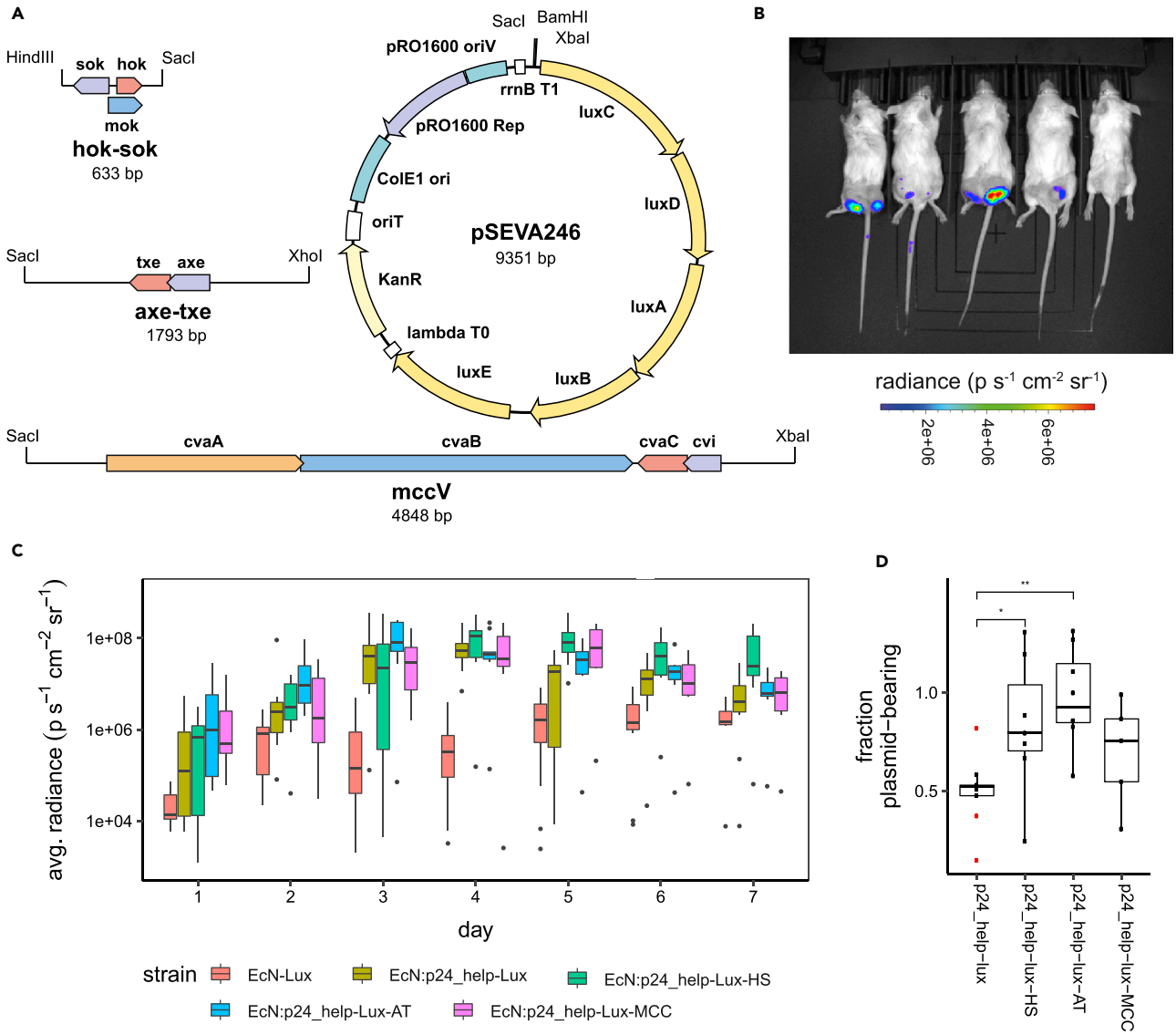

Figure 5. *In Vivo* Stability of Plasmid-Bearing EcN

(A) The plasmid stability systems were cloned into a plasmid using the constitutive help promoter to express luminescence genes.

(B) Representative image of plasmid-produced luminescence after bacterial colonization of implanted hind flank tumors.

(C) The luminescence was measured for each tumor, once a day for a week, showing colonization of the tumors by the bacterial strain and continued production of the recombinant luminescence genes. (Black circles show outliers.)

(D) Fraction of bacterial population remaining plasmid bearing 7 days after colonization, calculated from colony counts on selective and non-selective media performed in triplicate for each tumor. (Circles show samples, red circles are considered outliers. *p = 0.034, **p = 0.0013 in the Mann-Whitney U test for p24-Lux n = 9 tumors, p24-Lux-HS n = 7 tumors, p24-Lux-AT n = 8 tumors, p24-Lux-MCC n = 5 tumors.)

luminescence from the tumors in mice administered with the plasmid-bearing strains could be due to plasmid loss.

The tumors were then excised 7 days after injection, and a colony count was performed from the homogenized tissue to independently measure the stabilizing effect of the axe/txe, hok/sok, and microcin-V systems on the reporter construct. Figure 5D shows that without any stabilizing system ~50% of the population had dropped the p24-Lux plasmid after intravenous injection and tumor colonization. In comparison, the p24-Lux-AT was significantly stabilized (p = 0.0013) with nearly 100% of the population maintaining the plasmids after colonization. The strain p24-Lux-HS also showed significant stability over p24-Lux control (p = 0.034) with ~80% of the

population maintaining the plasmids after colonization. The bacteriocin plasmid p24-Lux-MCC did not show a significant improvement over the control, although the mean plasmid-bearing population was ~70%. There was also no significant difference between the plasmid-fraction-bearing population in p24-Lux-AT and p24-Lux-HS.

DISCUSSION

We developed an automated flow cytometry pipeline, mathematical model, and Bayesian inference procedure to quantify the efficacy of PSK systems stabilizing fluorescent and luminescent reporter constructs *in vitro* and *in vivo*. We used this pipeline to demonstrate that two new PSK systems in EcN, axe/txe and microcin-V, can outperform the more commonly used hok/sok system. Our method for Bayesian parameter estimation is able to accurately infer parameters from simulated data, and, where plasmid loss occurs, it can be used to estimate growth rate differences, plasmid loss rates, and PSK efficacy.

As expected, plasmids expressing fluorescent and luminescent proteins were shown to reduce the growth rate of EcN significantly, but there was minimal extra burden produced from the TA systems and a small burden from the bacteriocin system. Using four different plasmid origins of replication we have shown that plasmid copy number proportionally affects the growth rate of the plasmid-bearing strain. Here we have shown that the conventional wisdom, that lower copy number plasmids are less stable, is incorrect. Our mathematical model demonstrates that burden is an important consideration in plasmid stability. As such, any reduction in growth rate associated with higher copy number can prove more of a hindrance to plasmid maintenance than the increased chance of plasmid loss due to low plasmid copy number. Future work could include the use of whole-cell models to investigate how burden, copy number, and plasmid instability are related.

Our plasmid stability assays with both the fluorescent and luminescent plasmids showed that axe/txe provides greater plasmid stability than hok/sok. This is an interesting result as hok/sok is an *E. coli*-native TA system, whereas axe/txe was found in the gram-positive *E. faecium*. Furthermore, hok/sok is bactericidal (Faridani et al., 2006), whereas axe/txe is only bacteriostatic (Grady and Hayes, 2003). One might expect that the plasmid-free persister cells created from the txe toxin would begin to divide at a later passage and cause the plasmid-bearing population to become diluted, but this did not appear to happen during the 37 passages of the fluorescent strains.

The results for microcin-V show far more variability in plasmid stability than those for the TA systems. We have demonstrated that in those replicates in which plasmid loss was observed, plasmid-free cells had developed immunity to the bacteriocin. The similarity of microcin-V to bacteriocin systems already present in EcN 1917 may have made it simpler for such immunity to develop. However, there are a vast range of other bacteriocins to choose from that may well prove more reliable for prolonged applications.

Although microcin-V does not perform as well as axe/txe over the length of the plasmid stability experiments, we have shown that over a single passage of 24 h the bacteriocin is able to push a diluted population back to entirely plasmid bearing. For this reason, microcins may be particularly effective in industrial fermentation applications wherein the environment is relatively stable compared with the *in vivo* conditions encountered in clinical use.

A major focus of synthetic biology over the coming years will be to push proof-of-principle systems into real-world applications. A big limitation for industrial and clinical applications adopting synthetic biology tools is the use of antibiotic selection, and moving away from these laboratory-based systems will be critical. Our developed experimental and modeling approach can be used to characterize new systems for industrial applications and novel therapeutics. By inferring information about the relative growth rates and killing efficiency, a more quantitative viewpoint of plasmid stability mechanisms can be achieved, enabling the targeting of PSK systems to specific applications.

Limitation of Study

Our study contains two main limitations, which could be addressed with further work. (1) The mathematical model assumes constant plasmid copy number, within the plasmid-bearing population, during a passage, and between all passages. The average plasmid copy number at different time points within a passage has been shown to be dependent on the plasmid origin of replication (Jahn et al., 2016). It is, however, commonly known that adaptation between plasmid and host bacteria occurs after several generations (Bouma and Lenski, 1988) and that regulation of plasmid copy number may be involved. (2) Our modeling

also assumes no change in growth rate across passages, which due to the coevolution of plasmid and host, is likely to be an oversimplification as fitter cells are selected.

METHODS

All methods can be found in the accompanying Transparent Methods supplemental file.

DATA AND SOFTWARE AVAILABILITY

The data reported in this paper is available in Mendeley data.

SUPPLEMENTAL INFORMATION

Supplemental Information can be found online at https://doi.org/10.1016/j.isci.2019.03.019.

ACKNOWLEDGMENTS

We thank Professor Kenn Gerdes for sending the pKG1022 plasmid (now at the University of Copenhagen), Dr. Finbarr Hayes at The University of Manchester for sending the pREG531 plasmid, Professor Roberto Kolter at Harvard for the pHK11 plasmid, and Dr. Esteban Martinez-Garcia at CNB-CSIC for the SEVA plasmids. A.J.H.F is funded through the UCL CoMPLEX doctoral training center. T.O. was funded through the BBSRC LIDo doctoral training partnership. L.R. is funded jointly through a BBSRC studentship and a Microsoft Research Scholarship. Y.R. is funded by the BBSRC LIDo. Y.K.H. is funded by the BBSRC LIDo and by BBSRC (BB/N010221/1). V.B.P. would like to acknowledge BBSRC support (BB/K018132/1 and BB/N010221/1). T.D. was supported by an NIH R00 (CA197649) and DOD Era of Hope Award (BC160541). C.P.B. is supported through a Wellcome Trust Research Career Development Fellowship (097319/Z/11/Z). We thank C. Coker and J. Zhang in the Danino laboratory for assistance with mouse experiments.

AUTHOR CONTRIBUTIONS

T.O., A.J.H.F., and A.D. performed all plasmid cloning. A.J.H.F., T.O., L.R., and J.R. performed all *in vitro* plasmid loss experiments. Y.-K.H. carried out the qPCR experiments, which were conceived by A.J.H.F, Y.-K.H., and V.B.P. A.D. and O.V. performed the *in vivo* mouse model experiments. A.J.H.F. performed the population restoration experiments. A.J.H.F. and T.O. carried out the growth rate measurements. A.J.H.F. performed the bacteriocin immunity test. A.J.H.F. and C.P.B. undertook all modeling and fitting. A.J.H.F., T.O., and C.P.B. performed all further data analysis. A.J.H.F., T.O., T.D., and C.P.B. conceived this study, discussed results, and wrote the manuscript.

DECLARATION OF INTERESTS

The authors declare no competing interests.

Received: October 16, 2017
Revised: December 29, 2018
Accepted: March 18, 2019
Published: April 26, 2019

REFERENCES

Acuña, L., Corbalan, N.S., Fernandez-No, I.C., Morero, R.D., Barros-Velazquez, J., and Bellomio, A. (2015). Inhibitory effect of the hybrid bacteriocin ent35-mccv on the growth of Escherichia coli and listeria monocytogenes in model and food systems. Food Bioproc. Tech. *8*, 1063–1075.

Acuña, L., Picariello, G., Sesma, F., Morero, R.D., and Bellomio, A. (2012). A new hybrid bacteriocin, Ent35-MccV, displays antimicrobial activity against pathogenic Gram-positive and Gram-negative bacteria. FEBS Open Bio. *2*, 12–19.

Andrianantoandro, E., Basu, S., Karig, D.K., and Weiss, R. (2006). Synthetic biology: new engineering rules for an emerging discipline. Mol. Syst. Biol. *2*, 2006.0028.

Azpiroz, M.F., and Laviña, M. (2007). Modular structure of microcin H47 and colicin V. Antimicrob. Agents Chemother. *51*, 2412–2419.

Boe, L. (1996). Estimation of plasmid loss rates in bacterial populations with a reference to the reproducibility of stability experiments. Plasmid *36*, 161–167.

Boe, L., Gerdes, K., and Molin, S. (1987). Effects of genes exerting growth inhibition and plasmid stability on plasmid maintenance. J. Bacteriol. *169*, 4646–4650.

Boe, L., and Rasmussen, K.V. (1996). Suggestions as to quantitative measurements of plasmid loss. Plasmid *36*, 153–159.

Bouma, J.E., and Lenski, R.E. (1988). Evolution of a bacteria/plasmid association. Nature *335*, 351.

Campelo, A.B., Roces, C., Mohedano, M.L., Lpez, P., Rodrguez, A., and Martnez, B. (2014). A bacteriocin gene cluster able to enhance plasmid maintenance in Lactococcus lactis. Microb. Cell Fact. *13*, 77.

Casini, A., Storch, M., Baldwin, G.S., and Ellis, T. (2015). Bricks and blueprints: methods and standards for DNA assembly. Nat. Rev. Mol. Cell Biol. *16*, 568–576.

Cataudella, I., Trusina, A., Sneppen, K., Gerdes, K., and Mitarai, N. (2012). Conditional cooperativity in toxin-antitoxin regulation prevents random toxin activation and promotes fast translational recovery. Nucleic Acids Res. *40*, 6424–6434.

Danino, T., Prindle, A., Kwong, G.A., Skalak, M., Li, H., Allen, K., Hasty, J., and Bhatia, S.N. (2015). Programmable probiotics for detection of cancer in urine. Sci. Transl. Med. *7*, 289ra84.

Diago-Navarro, E., Hernndez-Arriaga, A.M., Kubik, S., Konieczny, I., and Daz-Orejas, R. (2013). Cleavage of the antitoxin of the pard toxin-antitoxin system is determined by the clpap protease and is modulated by the relative ratio of the toxin and the antitoxin. Plasmid *70*, 78–85.

Ellis, T., Adie, T., and Baldwin, G.S. (2011). DNA assembly for synthetic biology: from parts to pathways and beyond. Integr. Biol. (Camb). *3*, 109–118.

Faridani, O.R., Nikravesh, A., Pandey, D.P., Gerdes, K., and Good, L. (2006). Competitive inhibition of natural antisense Sok-RNA interactions activates Hok-mediated cell killing in Escherichia coli. Nucleic Acids Res. *34*, 5915–5922.

Feldgarden, M., and Riley, M.A. (1999). The phenotypic and fitness effects of colicin resistance in escherichia coli k-12. Evolution *53*, 1019–1027.

Ganusov, V.V., and Brilkov, A.V. (2002). Estimating the instability parameters of plasmid-bearing cells. I. Chemostat culture. J. Theor. Biol. *219*, 193–205.

Gerdes, K. (1988). The parB (hok/sok) locus of plasmid R1: a general purpose plasmid stabilization system. Nat. Biotechnol. *6*, 1402–1405.

Grady, R., and Hayes, F. (2003). AxeTxe, a broad-spectrum proteic toxinantitoxin system specified by a multidrug-resistant, clinical isolate of Enterococcus faecium. Mol. Microbiol. *47*, 1419–1432.

Grozdanov, L., Raasch, C., Schulze, J., Sonnenborn, U., Gottschalk, G., Hacker, J., and Dobrindt, U. (2004). Analysis of the genome structure of the nonpathogenic probiotic Escherichia coli strain Nissle 1917. J. Bacteriol. *186*, 5432–5441.

Inglis, R.F., Bayramoglu, B., Gillor, O., and Ackermann, M. (2013). The role of bacteriocins as selfish genetic elements. Biol. Lett. *9*, 20121173.

Jahn, M., Vorpahl, C., Hübschmann, T., Harms, H., and Müller, S. (2016). Copy number variability of expression plasmids determined by cell sorting and droplet digital pcr. Microb. Cell Fact. *15*, 211.

Kroll, J., Klinter, S., Schneider, C., Voß, I., and Steinbüchel, A. (2010). Plasmid addiction systems: perspectives and applications in biotechnology. Microb. Biotechnol. *3*, 634–657.

Lau, B.T., Malkus, P., and Paulsson, J. (2013). New quantitative methods for measuring plasmid loss rates reveal unexpected stability. Plasmid *70*, 353–361.

Lee, J.W., Gyorgy, A., Cameron, D.E., Pyenson, N., Choi, K.R., Way, J.C., Silver, P.A., Del Vecchio, D., and Collins, J.J. (2016). Creating single-copy genetic circuits. Mol. Cell *63*, 329–336.

Liu, T., Chen, J.-Y.Y., Zheng, Z., Wang, T.-H.H., and Chen, G.-Q.Q. (2005). Construction of highly efficient e. coli expression systems containing low oxygen induced promoter and partition region. Appl. Microbiol. Biotechnol. *68*, 346–354.

Loh, J.M., and Proft, T. (2013). Toxin-antitoxin-stabilized reporter plasmids for biophotonic imaging of group a streptococcus. Appl. Microbiol. Biotechnol. *97*, 9737–9745.

Martinez-Garcia, E., Aparicio, T., Goñi-Moreno, A., Fraile, S., and de Lorenzo, V. (2014). Seva 2.0: an update of the standard european vector architecture for de-/re-construction of bacterial functionalities. Nucleic Acids Res. *43*, D1183–D1189.

Moritz, E.M., and Hergenrother, P.J. (2007). Toxinantitoxin systems are ubiquitous and plasmid encoded in vancomycin-resistant enterococci. Proc. Natl. Acad. Sci. U S A *104*, 311–316.

Riedel, C.U., Monk, I.R., Casey, P.G., Morrissey, D., O'Sullivan, G.C., Tangney, M., Hill, C., and Gahan, C.G. (2007). Improved luciferase tagging system for listeria monocytogenes allows real-time monitoring in vivo and in vitro. Appl. Environ. Microbiol. *73*, 3091–3094.

Riley, M. (1998). Molecular mechanisms of bacteriocin evolution. Ann. Rev. Genet. *32*, 2552–2578.

Rosa, S.L.L., Casey, P.G., Hill, C., Diep, D.B., Nes, I.F., and Brede, D.A. (2013). In vivo assessment of growth and virulence gene expression during commensal and pathogenic lifestyles of luxABCDE-tagged enterococcus faecalis strains in murine gastrointestinal and intravenous infection models. Appl. Environ. Microbiol. *79*, 3986–3997.

Sassone-Corsi, M., Nuccio, S.-P., Liu, H., Hernandez, D., Vu, C.T., Takahashi, A.A., Edwards, R.A., and Raffatellu, M. (2016). Microcins mediate competition among Enterobacteriaceae in the inflamed gut. Nature *540*, 280–283.

Stecher, B., Denzler, R., Maier, L., Bernet, F., Sanders, M.J., Pickard, D.J., Barthel, M., Westendorf, A.M., Krogfelt, K.A., Walker, A.W., et al. (2012). Gut inflammation can boost horizontal gene transfer between pathogenic and commensal Enterobacteriaceae. Proc. Natl. Acad. Sci. U S A *109*, 1269–1274.

Summers, D. (1991). The kinetics of plasmid loss. Trends Biotechnol. *9*, 273–278.

Swain, P.S., Stevenson, K., Leary, A., Montano-Gutierrez, L.F., Clark, I.B.N., Vogel, J., and Pilizota, T. (2016). Inferring time derivatives including cell growth rates using Gaussian processes. Nat. Commun. *7*, 13766.

Theriot, C.M., Koenigsknecht, M.J., Carlson, P.E., Jr., Hatton, G.E., Nelson, A.M., Li, B., Huffnagle, G.B., Li, J., and Young, V.B. (2014). Antibiotic-induced shifts in the mouse gut microbiome and metabolome increase susceptibility to clostridium difficile infection. Nat. Commun. *5*, 3114.

Velur Selvamani, R.S., Friehs, K., and Flaschel, E. (2014a). Extracellular recombinant protein production under continuous culture conditions with Escherichia coli using an alternative plasmid selection mechanism. Bioproc. Biosyst. Eng. *37*, 401–413.

Velur Selvamani, R.S., Telaar, M., Friehs, K., and Flaschel, E. (2014b). Antibiotic-free segregational plasmid stabilization in Escherichia coli owing to the knockout of triosephosphate isomerase (tpia). Microb. Cell Fact. *13*, 58.

Wright, M.S., Baker-Austin, C., Lindell, A.H., Stepanauskas, R., Stokes, H.W., and McArthur, J.V. (2008). Influence of industrial contamination on mobile genetic elements: class 1 integron abundance and gene cassette structure in aquatic bacterial communities. ISME J. *2*, 417–428.

Wright, O., Stan, G.-B., and Ellis, T. (2013). Building-in biosafety for synthetic biology. Microbiology *159* (Pt 7), 1221–1235.

Yanisch-Perron, C., Vieira, J., and Messing, J. (1985). Improved m13 phage cloning vectors and host strains: nucleotide sequences of the m13mpl8 and puc19 vectors. Gene *33*, 103–119.

ISCI, Volume *14*

Supplemental Information

Two New Plasmid Post-segregational Killing Mechanisms for the Implementation of Synthetic Gene Networks in *Escherichia coli*

Alex J.H. Fedorec, Tanel Ozdemir, Anjali Doshi, Yan-Kay Ho, Luca Rosa, Jack Rutter, Oscar Velazquez, Vitor B. Pinheiro, Tal Danino, and Chris P. Barnes

1 Transparent Methods

Analytical Solutions to Plasmid Stability Models

Analytical solutions to the mathematical models in the main text were calculated using Mathematica (Wolfram Research, Inc. n.d.). The proportion of the population that is plasmid-bearing after τ plasmid-free generations can be written for the TA model as:

$$\begin{aligned}\phi_\tau(\lambda,\gamma,\omega) &= \frac{X^+(t)}{X^+(t)+X^-(t)} \\ &= \frac{e^{(\gamma-\gamma\lambda)\tau}}{\nu e^{\tau}+e^{(\gamma-\gamma\lambda)\tau}+\frac{(e^{\tau}-e^{(\gamma-\gamma\lambda)\tau})\gamma\lambda(1-\omega)}{1-\gamma+\gamma\lambda}}\end{aligned} \tag{1}$$

and for the bacteriocin model as:

$$\phi_\tau(\lambda,\gamma,\omega) = \frac{e^{(\gamma-\gamma\lambda)\tau}}{\nu e^{(1-2\omega)\tau}+e^{(\gamma-\gamma\lambda)\tau}+\frac{(e^{(1-2\omega)\tau}-e^{(\gamma-\gamma\lambda)\tau})\gamma\lambda}{1-\gamma+\gamma\lambda-2\omega}} \tag{2}$$

where $\nu = \frac{X^-(0)}{X^+(0)}$. For the plasmid loss experiments we assume that the initial population is entirely plasmid bearing i.e. $\nu = 0$.

Modelling Noise in Plasmid Loss Curves

The experimental method used to determine plasmid stability relies on sampling a population of cells and classifying each one as plasmid-bearing or plasmid-free. Every one of the n cells sampled is equivalent to a Bernoulli trial where "success" is a cell being plasmid-bearing and the probability parameter corresponds to the proportion of plasmid-bearing cells in the culture from which the sample was drawn. As such, a hypergeometric distribution can be used to describe the number of plasmid-bearing cells in any sample. However, since the fraction of the total population being sampled is very small, $\sim 1/5000$, a binomial model is a reasonable approximation:

$$X^+ \sim \text{Binomial}(n,\phi) \tag{3}$$

where n is the number of cells sampled and ϕ is the true proportion of plasmid-bearing cells in the population from which the sample was drawn.

The binomial model can describe the noise introduced in sampling the plasmid loss experiments but does not incorporate any intrinsic biological noise, which will result in overdispersion of the data. The "true proportion of plasmid-bearing cells", ϕ, from which the sample was taken, is the parameter that is effected by this biological noise. The uncertainty in this parameter is traditionally modelled using a beta distribution and the binomial and beta model can be combined into a beta-binomial model:

$$X^+ \sim \text{Beta-Binomial}\,(n,\alpha,\beta) \tag{4}$$

where

$$\alpha = \phi\left(\frac{1}{\rho}-1\right) \tag{5}$$

$$\beta = \frac{\alpha-\alpha\ \phi}{\phi} \tag{6}$$

thus the parameter ρ is used to reflect the uncertainty in ϕ. Simulated plasmid loss curves can be produced by sampling r replicates from the beta-binomial model at t timepoints. The plasmid-bearing population fraction is then given by:

$$\hat{\phi}_{r,t}(\lambda,\gamma,\omega,\rho,n) = \frac{X^+_{r,t}}{n} \tag{7}$$

where $X^+_{r,t}$ are r replicate samples at t timepoints from the beta-binomial distribution in Equation 4. ϕ in Equations 5 and 6, is generated at each timepoint using either the TA model in Equation 1 or the bacteriocin model in Equation 2. The effects of the sample size, n, and the uncertainty parameter, ρ, are shown in Supplementary Figure S22.

Strains and Plasmid Construction

Lysogeny broth (LB) media and agar was used during propagation and cloning of bacteria. Assays were carried out in LB media and when antibiotic selection was applied, kanamycin was used at 25 µg/mL and erythromycin at 100 µg/mL. All DNA manipulations were performed in *E. coli* DH5α (NEB) or *E. coli* Mach 1. All final plasmid stability assays were performed either in *E. coli* Nissle 1917 (EcN) or in *E. coli* Nissle 1917 with a genomically integrated erythromycin-resistant and *luxCDABE* cassette (EcN-Lux) (Danino et al. 2015) (Table S1).

Table S1: related to Figures 2-5. *E. coli* strains and plasmids used in this study.

Strain or plasmid	Description	Source
E. coli		
DH5α	Used for cloning.	New England BioLabs
Mach 1α	Used for cloning.	Invitrogen
EcN	*E. coli* Nissle 1917.	Prof. Ian Henderson, UK
EcN-Lux	*E. coli* Nissle 1917 with chromosomal *luxCDABE* and erythromycin resistance.	(Danino et al. 2015)
Plasmids		
pKG1022	A plasmid carrying hok/sok from pPR633.	(Gerdes 1988)
pREG531	A plasmid carrying axe/txe from pRUM.	(Grady & Hayes 2003)
pHK11	A plasmid carrying microcin-V from pColV-K30.	(Gilson et al. 1987)
pSEVA471	SC101 ori; SpR.	(Martinez-Garcia et al. 2014)
pSEVA261	p15A ori; KanR.	(Martinez-Garcia et al. 2014)
pSEVA246	Hybrid pRO1600/ColE1 ori; KanR; promoterless *luxCDABE*.	(Martinez-Garcia et al. 2014)
pUC-GFP	High copy pUC ori; KanR; 4540bp; constitutive daGFP expression under the strong OXB20 promoter.	Oxford Genetics
pUC-GFP-HS	pUC-GFP with hok/sok cassette.	This study
pUC-GFP-AT	pUC-GFP with axe/txe cassette.	This study
pUC-GFP-MCC	pUC-GFP with microcin-V cassette.	This study
pSC101-GFP	pUC-GFP with the pUC ori replaced with SC101 from pSEVA471.	This study
p15A-GFP	pUC-GFP with the pUC ori replaced with p15A from pSEVA261.	This study
pColE1-GFP	pUC-GFP with the pUC ori replaced with hybrid pRO1600/ColE1 ori from pSEVA246.	This study
pSC101-GFP-HS	pSC101-GFP with with hok/sok cassette.	This study
p15A-GFP-HS	p15A-GFP with hok/sok cassette.	This study
pColE1-GFP-HS	pColE1-GFP with hok/sok cassette.	This study
p24-Lux	pSEVA246 with phelp promoter in front of the *luxCDABE* operon.	This study
p24-Lux-HS	p24-Lux with hok/sok cassette.	This study
p24-Lux-AT	p24-Lux with axe/txe cassette.	This study
p24-Lux-MCC	p24-Lux with microcin-V cassette.	This study

Fluorescent assay plasmids were constructed using the pUC-GFP plasmid containing a pUC high copy origin-of-replication, a kanamycin resistance cassette and a dasher GFP gene being constitutively expressed in high quantities by the OXB20 promoter (Oxford Genetics, UK). The SC101, p15A and ColE1-RO1600 origins-of-replication were PCR amplified from their respective SEVA plasmids using the primers P.SEVA.ORI.F and P.PacI.SEVA.ORI.R. The fragments were digested using PacI and and FseI along with the pUC-GFP plasmid. The digested vector gel extracted to remove the band for the pUC origin and ligated with the new origin-of-replication fragments to create pSC101-GFP, p15A-GFP and pColE1-GFP.

Plasmid pUC-GFP-HS was created by ligating the 633bp HindIII to SacI fragment digested from pKG1022 (Gerdes 1988) into the MCS of pUC-GFP digested with the same restriction enzymes. Hok/sok was cloned into the other copy number plasmids in the same way. Plasmid pUC-GFP-AT was created by ligating the 1390bp BamHI to SacI fragment digested from pREG531 (Grady & Hayes 2003) into the MCS of pUC-GFP digested with the same restriction enzymes. Plasmid pUC-GFP-MCC was created by PCR amplification of pHK11 (Gilson et al. 1987) with primers P.SacI.mccV.FOR and P.XbaI.mccV.REV to amplify the microcin-V fragment with >400bp upstream and downstream of the annotated genes. This fragment was then digested with XbaI and SacI and ligated into pUC-GFP which had been digested using the same restriction enzymes. These plasmids were transformed into EcN-Lux using a standard thermal-shock transformation method to produce EcN-Lux:pUC-GFP, EcN-Lux:pUC-GFP-HS, EcN-Lux:pUC-GFP-AT, EcN-Lux:pUC-GFP-MCC (Table S1).

Luminescent assay plasmids were constructed from pSEVA246, a plasmid based on the SEVA architecture (Silva-Rocha et al. 2012, Martinez-Garcia et al. 2014) with a hybrid pRO1600/ColE1 high copy origin-of-replication, a kanamycin resistance cassette, and a multiple cloning site (MCS) upstream of a promoterless *luxCDABE* operon. The plasmids were produced in two steps. First the PSK systems were cloned into the MCS of plasmid pSEVA246. The hok/sok fragment was PCR amplified from pUC-GFP-HS with primers P.HS.SacI.F and P.HS.BamHI.R. This fragment was then digested with SacI and BamHI and ligated into pSEVA246 digested

Table S2: related to Figures 2-5. Primers used for the construction of plasmids. Underlined sequences show restriction sites added to the amplified fragments. Upper case letters show the annealing sequence.

Primer	Sequence
oris	
P.SEVA.ORI.F	CGGTGCTCAACGGGAATC
P.PacI.SEVA.ORI.R	cacaccttaattAAATCCGCCGCCCTAGAC
PSKs	
P.SacI.mccV.FOR	tgacgcgagctcTGCCCTTCCCTAGAGAATCC
P.XbaI.mccV.REV	actgtctctagaGGGTCAGTGCAGAATTTTTA
P.HS.SacI.F	atctgagagctcTCCGGCCGAACAAACTCC
P.HS.BamHI.R	atgtcaggatccAAGGAGAAAGGGGCTACCG

with the same enzymes. pUC-GFP-AT was digested with SacI and BamHI and the 1.3Kbp axe/txe fragment was ligated into pSEVA246 digested with the same enzymes. pUC-GFP-MCC was digested with SacI, XbaI and ApaLI; the third enzyme was added to cut the unwanted fragment and enable the gel extraction of the 4.8Kbp microcin-V fragment. This was ligated into pSEVA246 which had been digested with SacI and XbaI. The constitutive phelp promoter (Riedel et al. 2007) was cloned upstream of the *luxCDABE* cassette using Gibson assembly (Gibson et al. 2009). EcN was transformed individually with these plasmids via heat-shock methods to produce EcN:p24-Lux, EcN:p24-Lux-HS, EcN:p24-Lux-AT, EcN:p24-Lux-MCC (Table S1).

Growth Rate Assays

For fluorescent assay plasmids, overnight cultures of each strain were grown in selective LB media for 16 hours and diluted 1/1000 into 10 mL of non-selective LB media. 200 µL from each culture was then transferred into 6 wells of a black clear-bottom 96-well microtitre plate (Greiner Bio-one, Germany) and sealed with a Breathe-Easy sealing membrane (Sigma-Aldrich, UK). The plate was then grown in a shaking TECAN Spark microplate reader at 37°C for 20 hours with OD_{600} readings taken every 10 minutes. Growth curves were fitted using a non-parametric Gaussian process method (Swain et al. 2016). The same protocol was used for luminescent assay plasmids, however, due to the instability of the control luminescent plasmid (p24-Lux), kanamycin was added to the media for all of the plasmid-bearing strains in order to ensure the growth rates of plasmid-bearing bacteria were being measured. The luminescent assay plasmids were all compared to liquid cultures of EcN grown in plain LB media with no added antibiotics. The growth data and fits are shown in Supplementary Figures S3, S12 and S24.

qPCR Experiments to Determine Plasmid Copy Number

Calibration curves

Cultures of EcN-Lux and the four pUC-GFP based strains were grown overnight in 5 mL LB media with the appropriate antibiotics in 15 mL Falcon tubes. Cells were harvested from the overnight liquid cultures by centrifuging at 4C for 10 min at 4000 rpm. Supernatant was removed and cell pellet resuspended in a modified QuantiLyse buffer (10 mM Tris-HCl pH8.2, 100 µg mL^{-1} Proteinase K, 5 µM SDS (Pierce et al. 2002), with the addition of 1 mg mL^{-1} Lysozyme and 0.5 µg mL^{-1} Polymyxin B; QLP), a protease-based lysis buffer to extract DNA (genomic and plasmid) from cells. Resuspended cells were then further diluted with QLP buffer in 1:5 serial dilutions from 1/1 (neat) to 1/3125 of original cell content, to be used to generate qPCR standard curves. Samples were incubated at 37°C for 30 min, 50°C for 30 min, denatured at 95°C for 10 min, and held at 18°C.

The NEB Luna Universal qPCR Master Mix kit (#M3003) was used as per protocol (20 µL reactions), with 2 µL of each serial dilution sample as template DNA. Primers YKH341 (5- CAGGAGGCTTTCGCATGATTGA-3) and YKH342 (5- TCAGAGCAGCCGATTGTCTG-3) were used to amplify a 112bp portion of the aph(3)II (KanR) gene on the plasmid DNA (P), whilst primers YKH343 (5-GGTCAAGTCACCACCACTGT-3) and YKH344 (5-GCTCTTGTTCCATCTGGCGA-3) amplified a 121bp fragment spanning the terB-tus genes on the genomic DNA (G). qPCR of the serial dilutions of plasmid and genomic DNA was carried out on the LightCycler 480 Instrument II System, set to detect SYBR Green I (excitation at bandpass 465 nm, half band width 24 nm; detection at bandpass 510 nm, half band width 20 nm). The programme conditions are

Table S3: related to Figures 2 and 3. qPCR thermal program

	Target (°C)	Hold (mm:ss)	Ramp rate (°C s^{-1})
Denaturation			
	95	02:00	4.40
Quantification			
	95	00:15	1.00
	60	01:00	1.00
Melt curve			
	60	00:15	4.40
	95	-	0.03
Hold			
	40	00:30	2.20

separated into four stages, for initial denaturation of DNA, cycles of amplification and product/SYBR Green quantification, melt curve analysis, and a final holding step (Table S3).

Crossing point (Cp) values (the cycle at which the amplified sample fluorescence first rises above background fluorescence; typically when 10^{11} to 10^{12} molecules are present in the reaction; Roche Diagnostics GmbH, 2008) generated in the quantification stage are plotted against the $\log_{10}$ of dilution ratio values to generate standard curves for plasmid and genomic DNA (Supplementary Figure S25). The standard curves are used to identify an appropriate dilution ratio for subsequent qPCRs in amplifying plasmid and genomic DNA and for calculating PCR efficiency. PCR efficiency, E, was calculated from the gradient, m, of each standard curve with the equation $E = 10^{(-1/m)}$. While a standard curve with $m = -3.32$ would be a perfect amplification reaction with $E = 2$, often the reactions have inefficiencies. Genomic DNA amplification efficiency was 1.84, and plasmid DNA amplification efficiency was 1.88.

The melt curve analyses generated by the LightCycler 480 Software was used to check for specificity in product amplification. P amplicons are expected to have a melting temperature (Tm) of 85°C, whilst G amplicons have Tm=80°C. qPCR products were further run on 3% agarose, 1mM lithium acetate gels to verify the results from the melt curve analyses.

Plasmid loss confirmation

The wells of two 96-well microtitre plates were filled with 200 µL of LB media with erythromycin. In the first plate, each of the wells was inoculated from glycerol stocks of the strains used to inoculate the initial plate for the plasmid stability assay, producing six replicates of each strain. In the second plate, each of the wells was inoculated from glycerol stocks made at the 30th passage of the plasmid stability assay. These plates were sealed with Breathe-Easy sealing membranes (Diversified Biotech) and incubated at 37°C for 16 hours with continuous shaking.

As before, cells were harvested by centrifuging at 4°C for 10 min at 4000 rpm, the supernatant was removed, and the pellets were resuspended in QLP buffer. Samples were diluted down to 1/25 of original cell content, and used as template with the NEB Luna Universal qPCR Master Mix kit (#M3003), as described previously. Again, all qPCR products were run on 3% agarose, 1mM lithium acetate gels to verify qPCR product specificity.

The average plasmid copy number was calculate using the expression

$$n = \frac{E_G^{Cp_G}}{E_P^{Cp_P}} \tag{8}$$

where E_G and E_P are amplification efficiencies of the genomic and plasmid PCRs and Cp_G and Cp_P are the crossing point values determined for each sample.

Plasmid copy number determination

Cultures of each of the strains containing the plasmids with different origins of replication were grown overnight in 5 mL LB media with erythromycin and kanamycin in 15 mL Falcon tubes. The wells of a 96-well microtitre plate were filled with 200 µL of LB media with erythromycin and kanamycin. Each of the wells was inoculated with 1 µL from the overnight cultures, for a total of six replicates per strain. The plate was sealed with a Breathe-Easy sealing membrane and incubated at 37°C for 16 hours with continuous shaking. The plate was then treated as above to determine average plasmid copy number for each well.

Plasmid Stability Assays in Liquid Culture

Assays were performed in LB media in sterile deep square 96-well (2.2mL) polypropylene plate. The edge wells were used for LB media controls so that the strains weren't affected by any potential plate edge conditions (Hall et al. 2013). The 96-well plate was split into two sections; one section with 500mL LB media containing erythromycin (100µg/mL) and kanamycin (25 µg/mL) and the second with LB media containing only erythromycin The erythromycin was used to prevent external contamination as the resistance gene is encoded on the chromosome of the EcN-Lux bacterial strain. The kanamycin is used to ensure plasmid maintenance, generating a plasmid-bearing control throughout the experiment.

For the plasmid stability assay with various PSK mechanisms based on the fluorescent reporter plasmid, three double selective wells for each strain (EcN-Lux:pUC-GFP, EcN-Lux:pUC-GFP-HS, EcN-Lux:pUC-GFP-AT, EcN-Lux:pUC-GFP-MCC) were inoculated by picking single colonies from selective LB agar plates. Six single selective wells were inoculated with EcN-Lux, as a plasmid-free control, by picking single colonies from selective LB agar plates. The plate was covered with a System Duetz breathable silicon sandwich (EnzyScreen, The Netherlands) and clamped down in a shaking incubator at 37°C and 350 rpm for 24 hours. This produced the time point 0 cultures. These cultures were then used to inoculate 1:500 a fresh plate, arranged with the same selective layout. Each double selective culture was used to inoculate 3 replicates for the assay of PSK systems in single selective media. This produced 9 replicates of each plasmid-bearing strain in single selective media and 3 in double selective media. The EcN-Lux plasmid-free control had 6 replicates in single selective media. Although the double selective media was inoculated with the EcN-Lux strain, as expected, no bacteria grew. This plate was covered and incubated as before. For subsequent passages the plate was replicated 1:500 into fresh media with a one-to-one mapping between wells.

At each passage, 200 µL of the overnight culture was transferred into a black clear-bottom 96-well microtitre plate (Greiner Bio-one, Germany) and absorbance (600 nm), fluorescence (ex=480 nm, em=540 nm), and luminescence were measured in a microplate reader. In addition, 1 µL of the overnight culture was transferred into a round-bottom 96-well microtitre plate containing 200 µL of PBS and the single cell fluorescence was measured using a flow cytometer.

For the plasmid stability assay with various PSK mechanisms based on the luminescent reporter plasmid, the assay was carried out as above but the initial inoculations were with the luminescent strains (EcN:p24-Lux, EcN:p24-Lux-HS, EcN:p24-Lux-AT, EcN:p24-Lux-MCC) and the plasmid free control was EcN rather than EcN-Lux. Furthermore, the assays could not be performed with erythromycin as the EcN bacterial host did not contain the resistance gene. In order to prevent external contamination in LB cultures without any antibiotic, the entire plate was additionally exposed to UV light for 40 minutes before inoculation at each passage (Sharma 2012). Further, only absorbance and luminescence could be measured so the preparation of the plate for flow cytometry was not carried out. Absorbance was additionally measured at 410nm.

For the plasmid stability assay with various origins-of-replication, the assay was performed as with the fluorescent PSK plasmids. The initial inoculations were with strains EcN-Lux:pUC-GFP, EcN-Lux:pUC-GFP-HS, EcN-Lux:pSC101-GFP, EcN-Lux:pSC101-GFP-HS, EcN-Lux:p15A-GFP, EcN-Lux:p15A-GFP-HS, EcN-Lux:pColE1-GFP, EcN-Lux:pColE1-GFP-HS into double selective media and the plasmid free control was EcN-Lux. Due to the larger number of strains, each double selective culture was used to inoculate 2 replicates rather than 3.

Flow Cytometry Data Processing

In order to ensure the capture of all bacterial events during flow cytometry sampling, a threshold was used that also captured a considerable amount of non-bacterial events. This can be problematic as the small size of bacteria leads to the bacterial population appearing very close to this debris. A further problem is that more than one bacterium can be read as a single event due to clumping. A computational pipeline was developed to automate the gating of singlet bacteria while excluding background debris and bacterial doublets. This process is important to automate as it removes operator bias associated with the manual drawing of gates and speeds up the analysis when large numbers of samples are recorded.

The method fits two dimensional mixture models of one and two clusters to the forward-scatter-height and side-scatter-height variables with 95% confidence. Using integrated completed likelihood (ICL) (Biernacki et al. 2000) the number of clusters that best fits the data is determined. This allows for compatibility with experiments in which debris has been removed by hand by an experimenter or if not many debris events are recorded. For any clusters found, their median positions are determined and if a cluster is below a pre-determined threshold it is considered debris and removed.

Doublets are then removed in one of two ways. Initially, a linear model was fitted to the side-scatter-height

versus side-scatter-area data and points falling too far away were removed as doublets. An update to the Attune NxT software implemented area scaling which is calibrated automatically during the start-up procedure. The area scaling allows the assumption that singlets will lie on, or close to, the line side-scatter-height = side-scatter-area. As such, for later experiments this method is used for doublet discrimination.

The output from this processing are standard flow cytometry .fcs files with debris and doublets removed. The software, written in R, for performing this analysis can be found at https://github.com/ucl-cssb/autoGate.

Hierarchical Bayesian Model Fitting to Plasmid Loss Curves

The models detailed by Equations 1 and 2 are fitted to the experimental plasmid loss curves using a hierarchical Bayesian model.

From the plasmid loss experiments, at each timepoint, t, there are r replicates for which analysis of the flow cytometry data produces the number of plasmid-bearing cells $X^+_{r,t}$ in a sample of size $n_{r,t}$. Note that the sample size varies for each sample as all cells within a specified volume are measured rather than cutting off after a given number of events have been recorded.

The aim here is to determine the set of model parameters, $\{\lambda, \gamma, \omega\}$, and noise parameter, ρ, which are most likely to produce the data observed using flow cytometry. To do so we build a hierarchical model for the three plasmid loss model parameters, Supplementary Figure S23. In this model, the log of the plasmid loss probability, λ, has a global distribution for all strains with plasmids based on the same backbone. The posterior distribution for this global λ is determined by sampling from a uniform prior, $U(-10, 0)$ and the posterior distribution for the standard deviation, σ^λ, in the global λ is sampled from an exponential prior, $Exp(100)$, which produces a shrinkage pressure on the distribution. Below the global level, there is a distribution on λ for each strain, sampled from a normal distribution with a mean sampled from the global distribution on λ and a standard deviation sampled from the global distribution on σ^λ. There is a strain level standard deviation on the strain level λ which is sampled from an exponential prior in the same manner as the global one. Finally, at the lowest level, each replicate of a strain has a posterior distribution on λ which is sampled from a normal distribution with mean sampled from the strain level λ and standard deviation sampled from the strain level standard deviation.

Since the growth rates of each strain can be directly measured, strain level distributions for the growth ratio parameter, γ, can be directly determined. As such, the replicate level posterior distributions for γ are sampled from a normal distribution with mean sampled from the strain level γ and standard deviation given by the standard deviation of the strain level γ.

The parameter encapsulating the efficacy of the killing mechanisms, ω, cannot be said to be globally linked. This is particularly true when considering the differences between the bacteriocin and TA systems but also applies between different TA systems as they function in distinct ways. As such, each strain has a posterior distribution on ω and standard deviation sampled from uniform priors. Each replicate then has a posterior distribution on ω sampled from a normal distribution with mean and standard deviation sampled from the the strain level ω and standard deviation.

The fitting is performed for all data for all strains concurrently using Rstan, the R language version of stan (Carpenter et al. 2016). As such, the log likelihood can be written as:

$$L(\theta|\mathbf{X}^+) = \sum^{s}\sum^{r}\sum^{t} \log\left(P\left(X^+_{s,r,t}|\theta\right)\right) \tag{9}$$

where θ is the full set of parameters, $\{\lambda_{s,r}, \lambda_s, \sigma^\lambda_s, \lambda, \sigma^\lambda, \gamma_{s,r}, \gamma_s, \sigma^\gamma_s, \omega_{s,r}, \omega_s, \sigma^\omega_s, \rho_{s,r}\}$ and:

$$\begin{aligned}
P(X^+_{s,r,t}|\theta) &= \text{Beta-Binomial}\left(n_{s,r,t}, \alpha_{s,r,t}, \beta_{s,r,t}\right) \\
\alpha_{s,r,t} &= \phi_{s,r,t}\left(\lambda_{s,r}, \gamma_{s,r}, \omega_{s,r}\right)\left(\frac{1}{\rho_{s,r}} - 1\right) \\
\beta_{s,r,t} &= \frac{\alpha_{s,r,t} - \alpha_{s,r,t}\ \phi_{s,r,t}\left(\lambda_{s,r}, \gamma_{s,r}, \omega_{s,r}\right)}{\phi_{s,r,t}\left(\lambda_{s,r}, \gamma_{s,r}, \omega_{s,r}\right)}
\end{aligned}$$

This hierarchical method of fitting can be demonstrated using simulated data of two strains, with and without PSK. Both of these data sets are simulated using the same plasmid loss probability, λ, growth rate ratio, γ, and noise, ρ. The difference is in the PSK efficacy parameter, ω. Supplementary Figure S2 shows the model fit to the full set of timecourses for each simulated strain, using the strain level parameter posteriors.

Plasmid-bearing Strain Dilution Assays

Starter cultures were produced in the same way as for the plasmid stability assays. Different dilutions of plasmid-bearing to plasmid-free strains were then produced by pipetting different volumes of plasmid-bearing overnight culture into EcN-Lux overnight culture in percentages from 10% through to 100%, keeping a total volume of 100 µL. For example, to produce a 30% culture 30 µL of plasmid-bearing overnight culture was added to 70 µL of EcN-Lux overnight culture. Note that the overnight cultures were not normalised to the same optical density, so a 30% culture does not mean that 30% of the cells are plasmid-bearing. Assays were performed in LB media in sterile autoclaved deep square 96-well (2.2mL) polypropylene plate. Each well was filled with 500 µL of LB media with erythromycin (100 µg/mL). The wells were then inoculated in a random pattern with 3 replicates of each of the diluted cultures. At the same time a 96-well mictrotitre plate was prepared with 200 µL of PBS in each well and inoculated from the same diluted cultures and measured using the same flow cytometry set up as above. The deep well plate was then sealed and incubated as above. After 24 hours the plate was taken from the incubator and passaged while a flow cytometry plate was also prepared and measured. This was carried out for a total of 2 passages. We used the data from passage 1-2 for the model fitting as this allowed the cells time to get used to growing in the deep-well plate. However, for the MCC strain we had to use data for passage 0-1 because after 24 hours all plasmid-free bacteria had been killed.

Luminescent Plasmid Stability Assays *in vivo*

All animal work was approved by the institutional committee on animal care (Columbia, AC-AAAN8002). The protocol requires animals to be euthanized when tumours reach 2 cm^3, or under veterinary staff recommendation. The cell line (MC26-LucF, Tanabe laboratory, Massachusetts General Hospital) was obtained from, and authenticated by, the Tanabe laboratory, MGH. The cell line was tested to be mycoplasma-free before implantation in mice. Sample sizes for mice were determined by expected effect size to produce a power of 0.8-0.9. Mice were blindly randomized into various groups using a random number generator.

Animal experiments were performed on 6-week-old female BALB/c mice (Taconic Biosciences) with bilateral subcutaneous hind flank tumours from an implanted mouse colon cancer cell line (MC26-LucF). The concentration for implantation of the tumour cells was 10^8 cells per ml in DMEM (no phenol red). Cells were then implanted subcutaneously at a volume of 100 µL per flank, with each implant consisting of 10^7 cells. The MC26 cells where given 14 days to graft and grow until they reached a size of approximately 150-200 mm^3. Along with an EcN-Lux strain as a control, EcN:p24-Lux, EcN:p24-Lux-HS, EcN:p24-Lux-AT and EcN:p24-Lux-MCC were grown up in LB with kanamycin until exponential phase, washed three times in sterile PBS and then injected intravenously at a dosage of $1x10^6$ bacteria in 100 µL. After bacterial colonisation of the tumours, animals were monitored via IVIS (IVIS 200, Caliper Life Sciences) to detect the presence of the plasmid via bioluminescence. Briefly, this involved anaesthetising the mice with isoflurane and imaging with an open filter on the auto-exposure setting. After 7 days, each of the tumours were sterilely extracted and homogenised using a tissue dissociator (Miltenyi), an aliquot of which was seeded on each of LB plates and LB with kanamycin plates. The ratio was calculated by comparing the mean counts of plasmid bearing colonies on LB plates and LB plates with kanamycin from each tumour (Danino et al. 2015). ggplot2 package in R was used for plotting. Statistical significance was demonstrated by the Mann-Whitney U test with R.

Bacteriocin Resistance Check

The wells of a 96-well microtitre plate was filled with 200 µL of LB media, half with erythromycin and half with erythromycin and kanamycin. The wells of this plate were inoculated with 1 µL of each of the EcN-Lux:pUC-GFP-MCC wells from a glycerol stock of the 30th passage of the plasmid loss experiment, replicated so that there was a sample of each well growing under each selective condition. Additionally, wells of EcN-Lux and a control EcN-Lux:pUC-GFP-MCC were inoculated under each selective condition. This plate was then sealed with a Breathe-Easy membrane and grown at 37 °C in a shaking plate reader for 6 hours. 1 µL from each of the wells was then spotted onto an LB agar plate, also containing erythromycin. Next to each of the cultures grown in LB+Er was spotted 1 µL of the control EcN-Lux:pUC-GFP-MCC, grown in LB+Er. Next to each of the cultures grown in LB+Er+Kn was spotted 1 µL of EcN-Lux grown in LB+Er. The left to dry until the spots were no longer visibly wet. The plate was then placed in an incubator at 37 °C fro 16 hours. After incubation, images of the plate were taken on a blue light transilluminator with amber filter (IORodeo), to record GFP fluorescence, and using a gel documentation system with UV transillumination, to visualise colony growth (Supplementary Figure S19).

2 Supplementary Figures

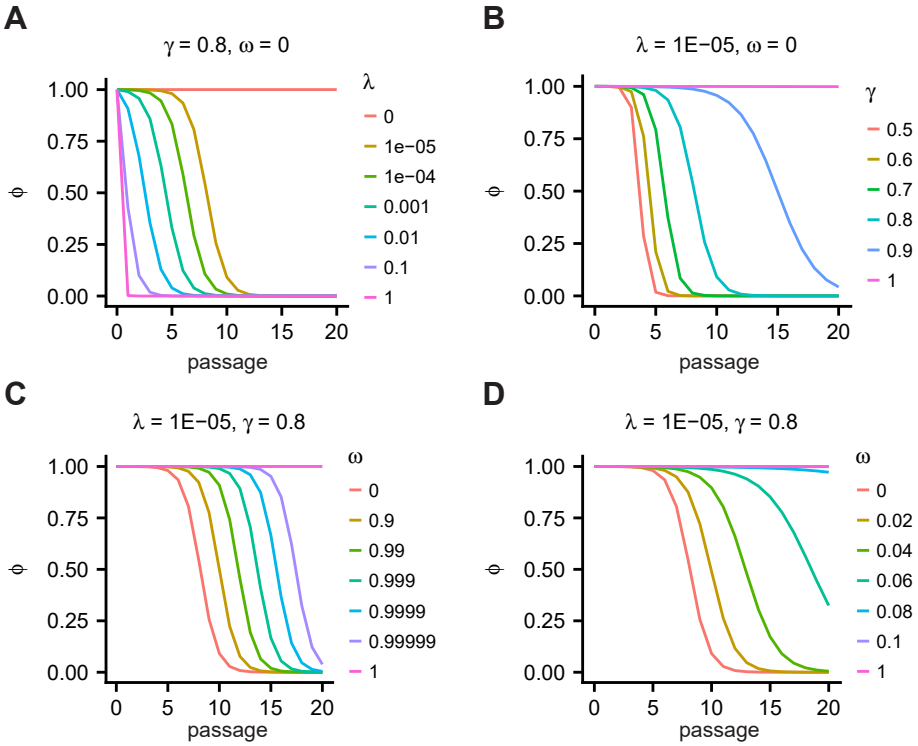

Figure S1: related to Figures 3 and 4. Effects of model parameters on plasmid-loss curves. A) Varying the plasmid loss probability, λ, and B) the doubling time ratio, γ, without post-segregational killing or bacteriocin killing. These are identical for the TA and the bacteriocin models when $\omega = 0$. C) Varying the efficacy of the toxin, ω, in the TA model. D) Varying the efficacy of the bacteriocin, ω, in the bacteriocin model.

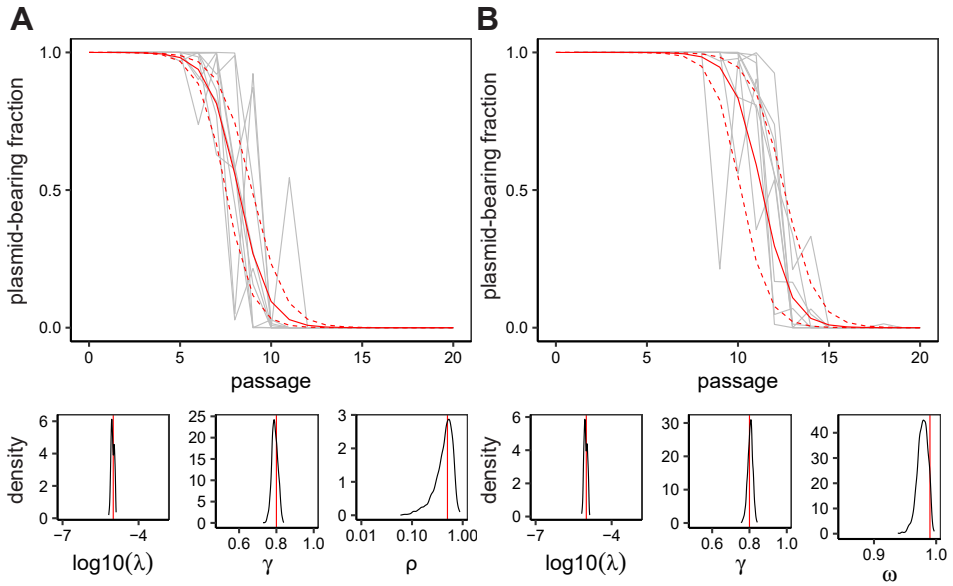

Figure S2: related to Figure 3. Fits of the hierarchical model at the strain level to simulated plasmid loss curves A) without PSK and B) with PSK. The grey lines show the nine simulated trajectories, the solid red line shows the mean model fit and the dashed lines show the 95% confidence intervals. Since the ω parameter is not relevant to the fitting of the timecourses without PSK, the posterior distribution of the noise parameter ρ is shown below the plasmid loss curve of (A) instead.

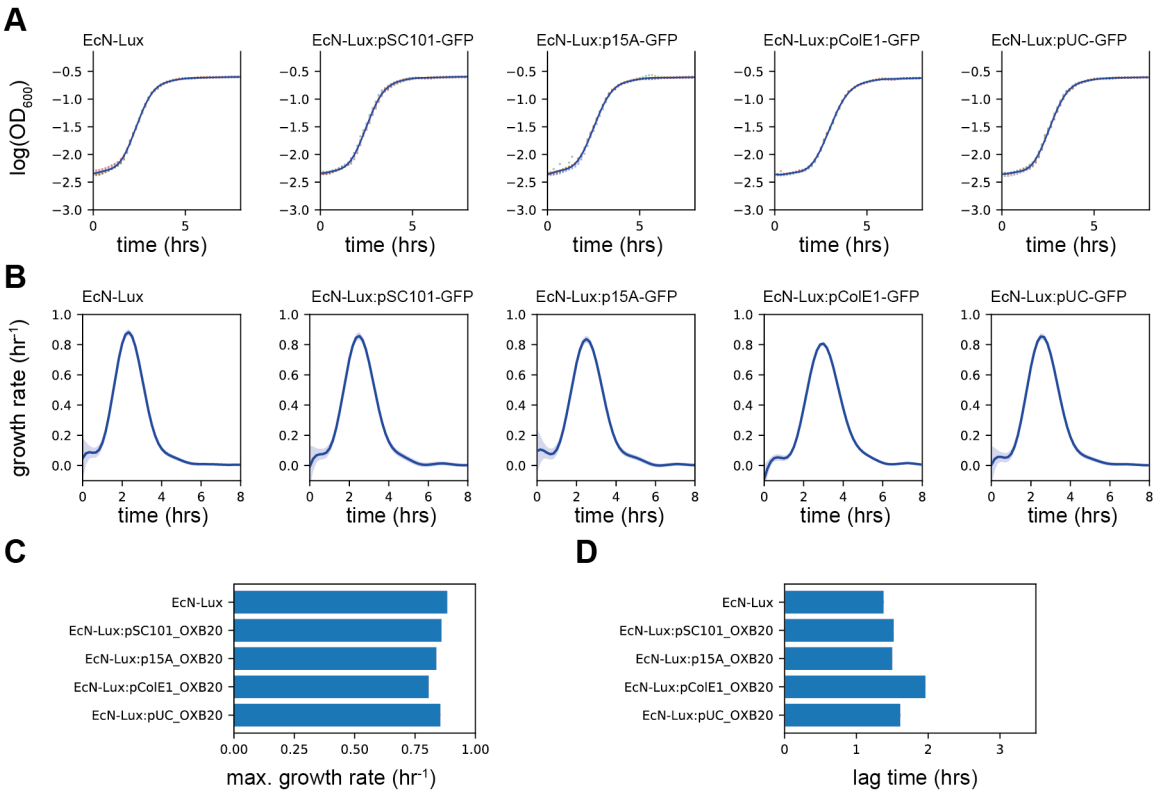

Figure S3: related to Figure 2. Growth curves and model fits for the fluorescent plasmids with different origins-of-replication in EcN-Lux grown in LB media with erythromycin. (A) Logged optical density measured at 600nm. The points show 6 replicates for each strain with the different colours indicating each replicate. The blue line shows the non-parametric Gaussian process fit with standard error shown by the light blue area around the line. (B) Estimated growth rate as a function of time. (C) Estimated maximal growth rates and (D) estimated lag time. The red lines show the standard deviation of the mean.

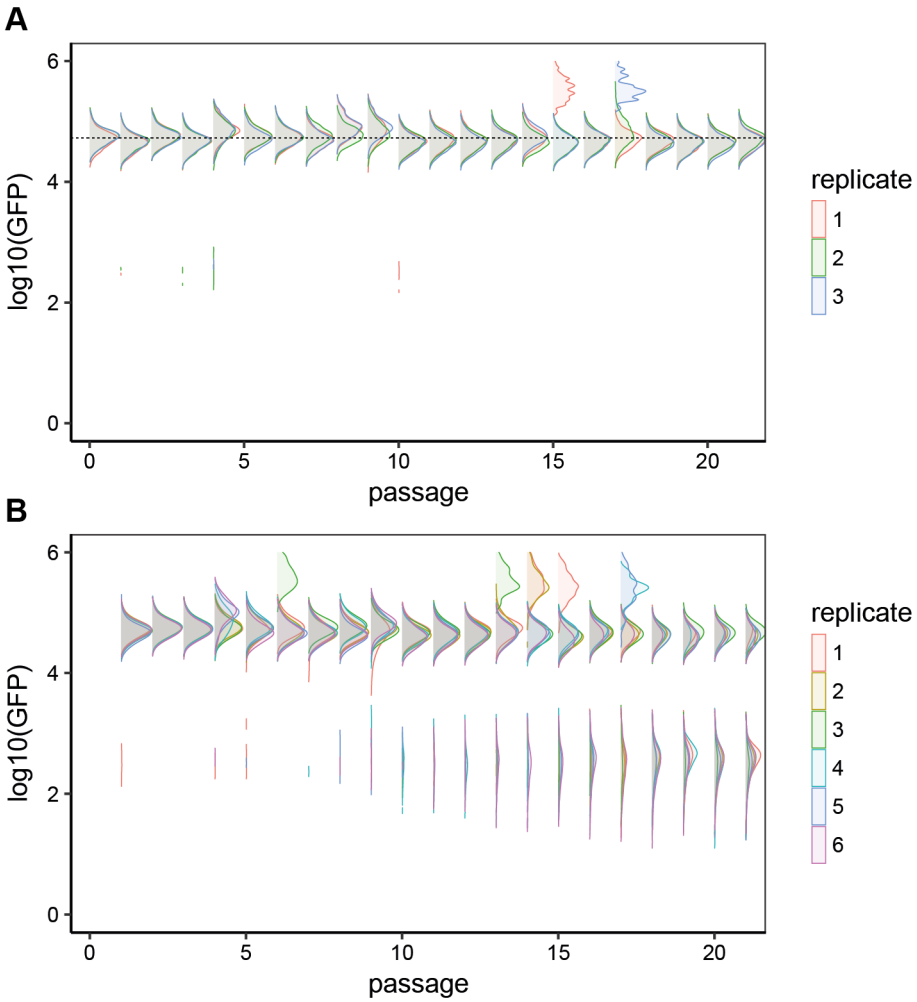

Figure S4: related to Figure 2. Flow cytometry samples of EcN-Lux:pSC101-GFP. A) 3 replicates grown in LB media with erythromycin and kanamycin, ensuring plasmid maintenance. The black dashed line indicates the median fluorescence at passage 0. B) 6 replicates grown in LB media with erythromycin only, allowing for plasmid loss.

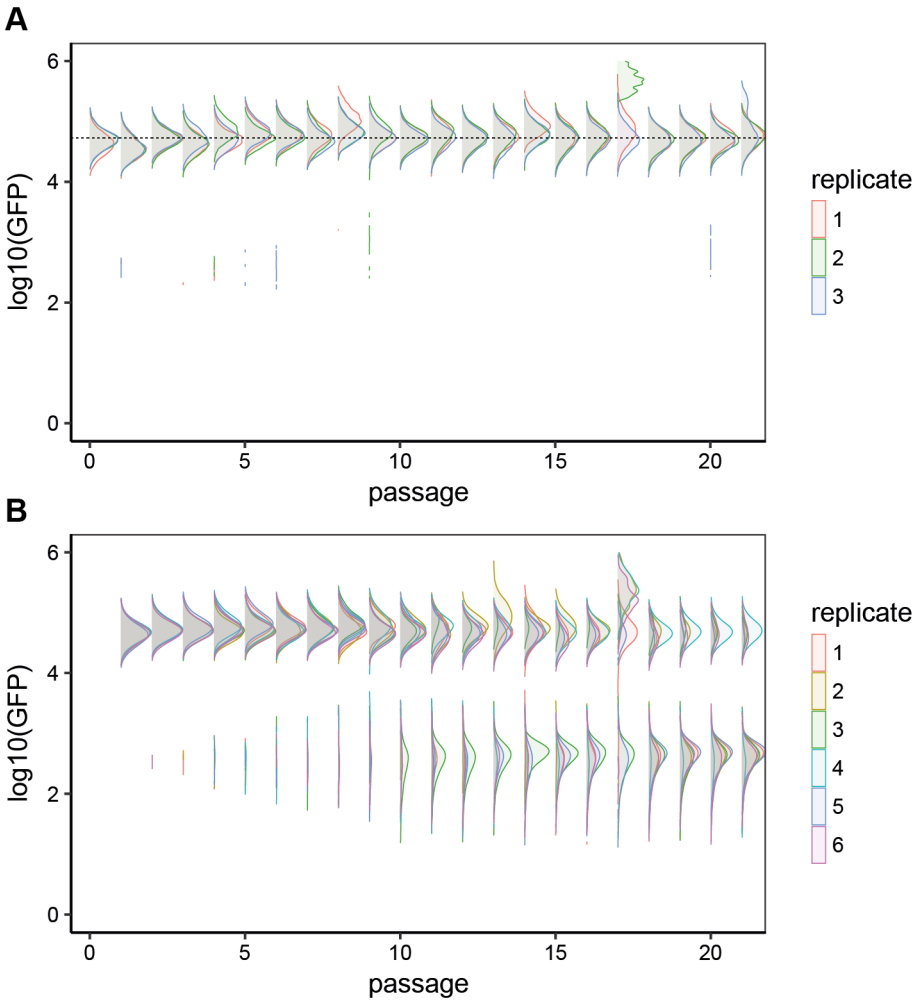

Figure S5: related to Figure 2. Flow cytometry samples of EcN-Lux:p15A-GFP. A) 3 replicates grown in LB media with erythromycin and kanamycin, ensuring plasmid maintenance. The black dashed line indicates the median fluorescence at passage 0. B) 6 replicates grown in LB media with erythromycin only, allowing for plasmid loss.

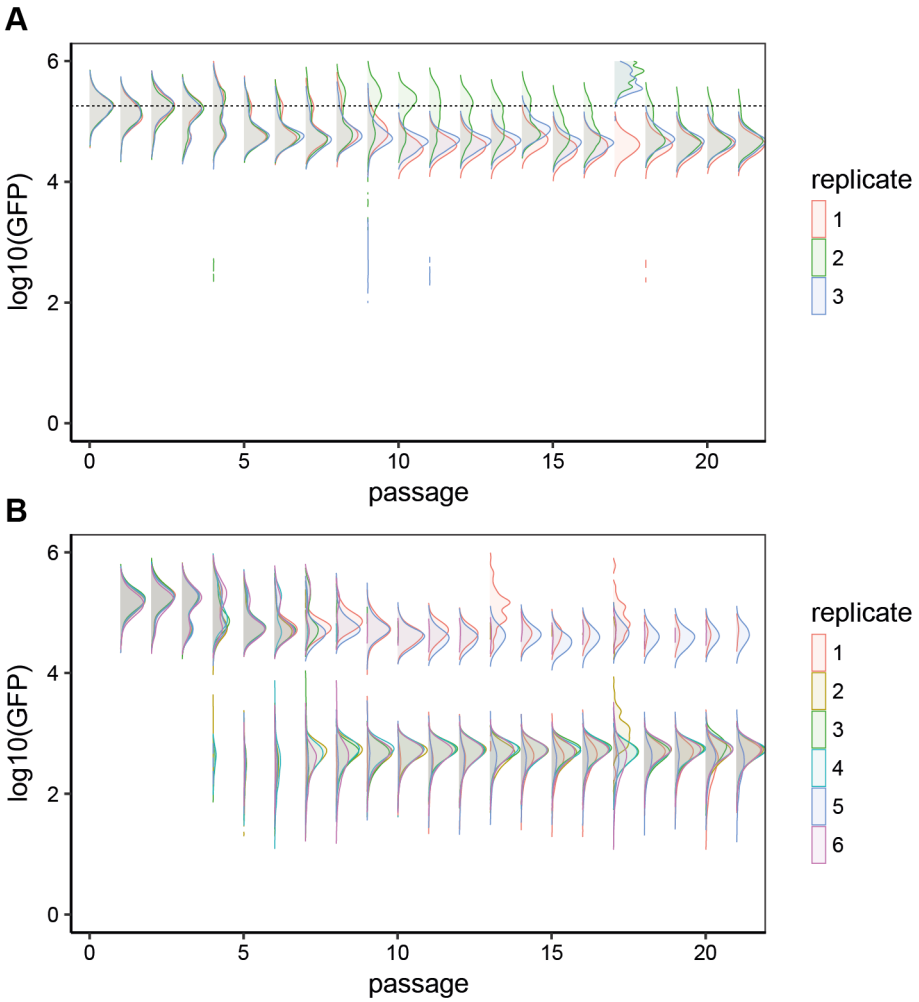

Figure S6: related to Figure 2. Flow cytometry samples of EcN-Lux:ColE1-GFP. A) 3 replicates grown in LB media with erythromycin and kanamycin, ensuring plasmid maintenance. The black dashed line indicates the median fluorescence at passage 0. B) 6 replicates grown in LB media with erythromycin only, allowing for plasmid loss.

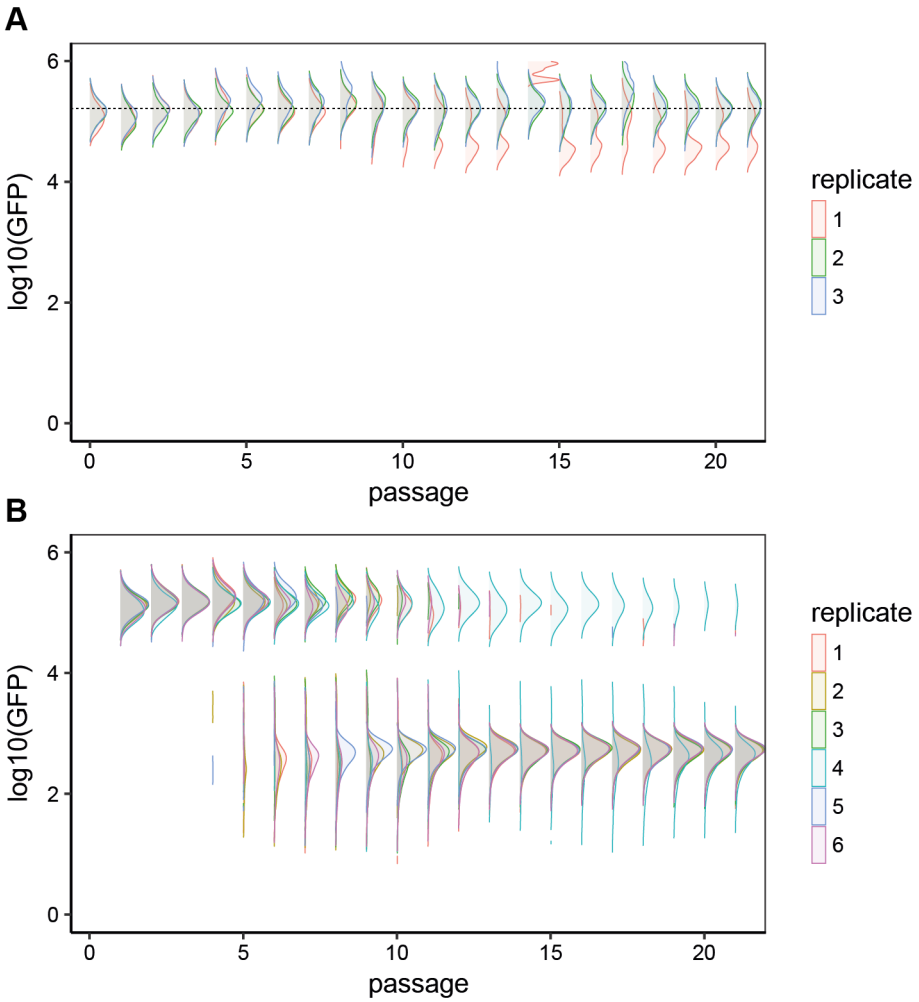

Figure S7: related to Figure 2. Flow cytometry samples of EcN-Lux:pUC-GFP. A) 3 replicates grown in LB media with erythromycin and kanamycin, ensuring plasmid maintenance. The black dashed line indicates the median fluorescence at passage 0. B) 6 replicates grown in LB media with erythromycin only, allowing for plasmid loss.

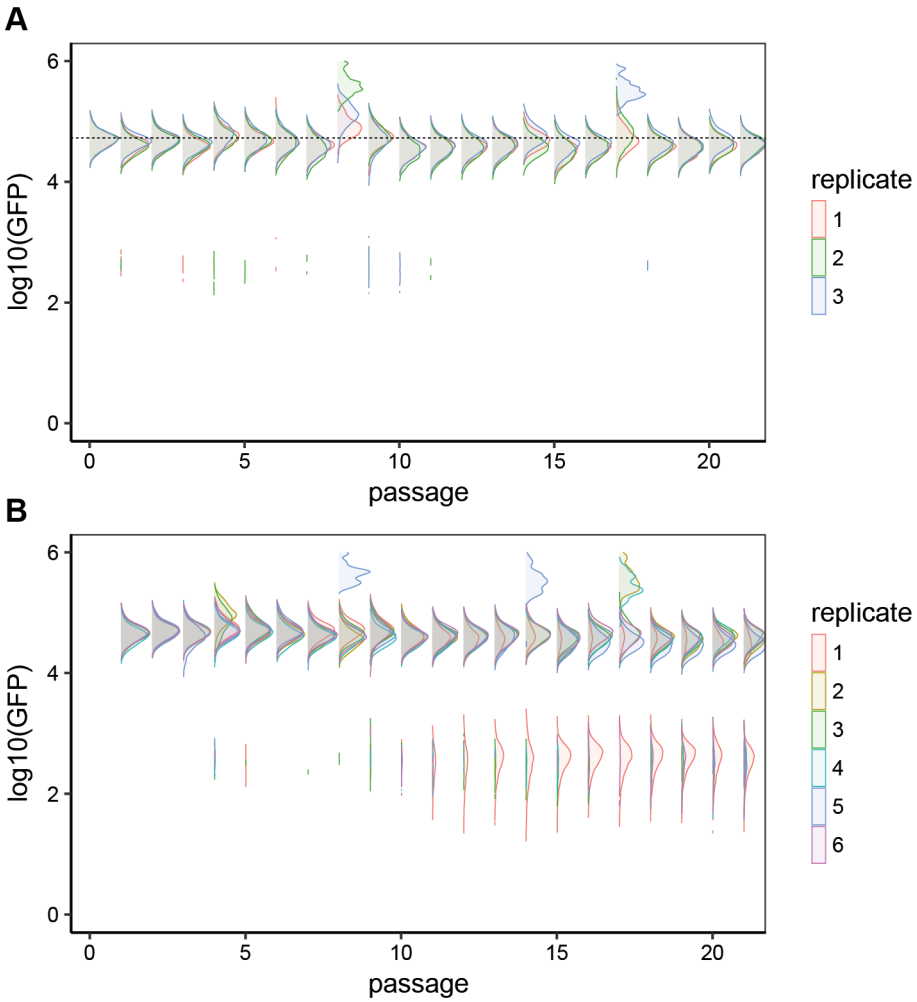

Figure S8: related to Figure 2. Flow cytometry samples of EcN-Lux:pSC101-GFP-HS. A) 3 replicates grown in LB media with erythromycin and kanamycin, ensuring plasmid maintenance. The black dashed line indicates the median fluorescence at passage 0. B) 6 replicates grown in LB media with erythromycin only, allowing for plasmid loss.

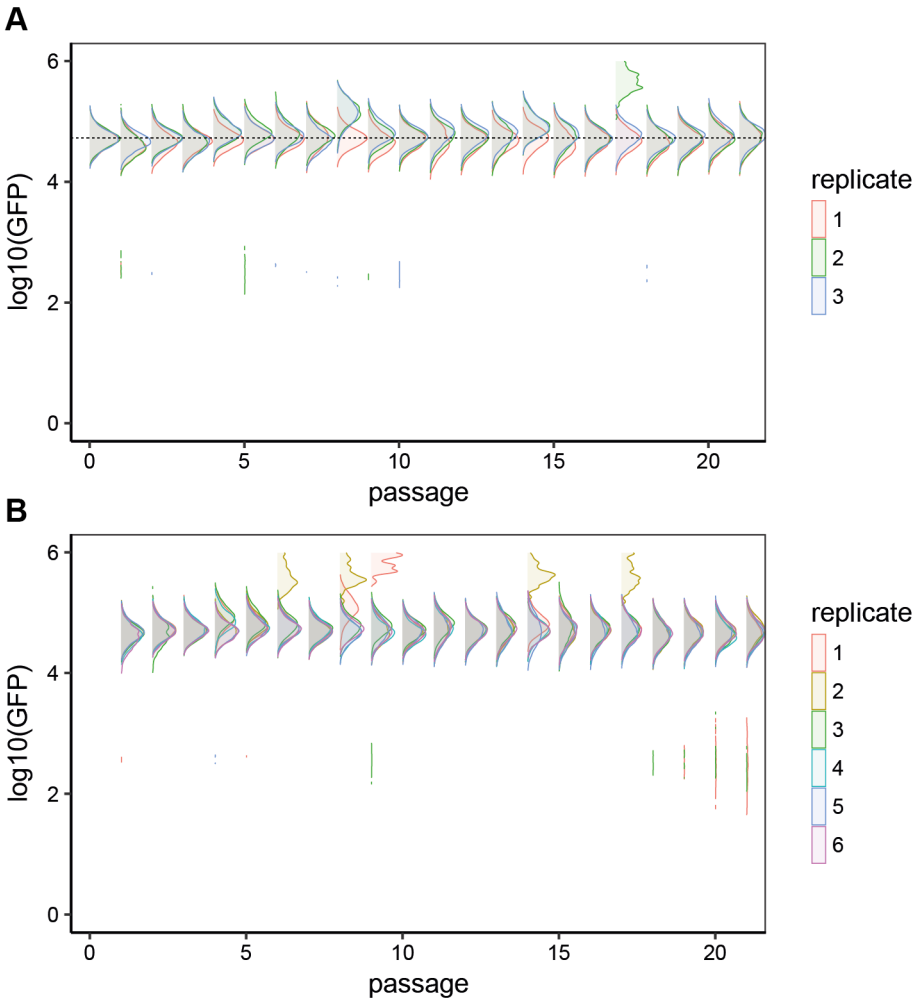

Figure S9: related to Figure 2. Flow cytometry samples of EcN-Lux:p15A-GFP-HS. A) 3 replicates grown in LB media with erythromycin and kanamycin, ensuring plasmid maintenance. The black dashed line indicates the median fluorescence at passage 0. B) 6 replicates grown in LB media with erythromycin only, allowing for plasmid loss.

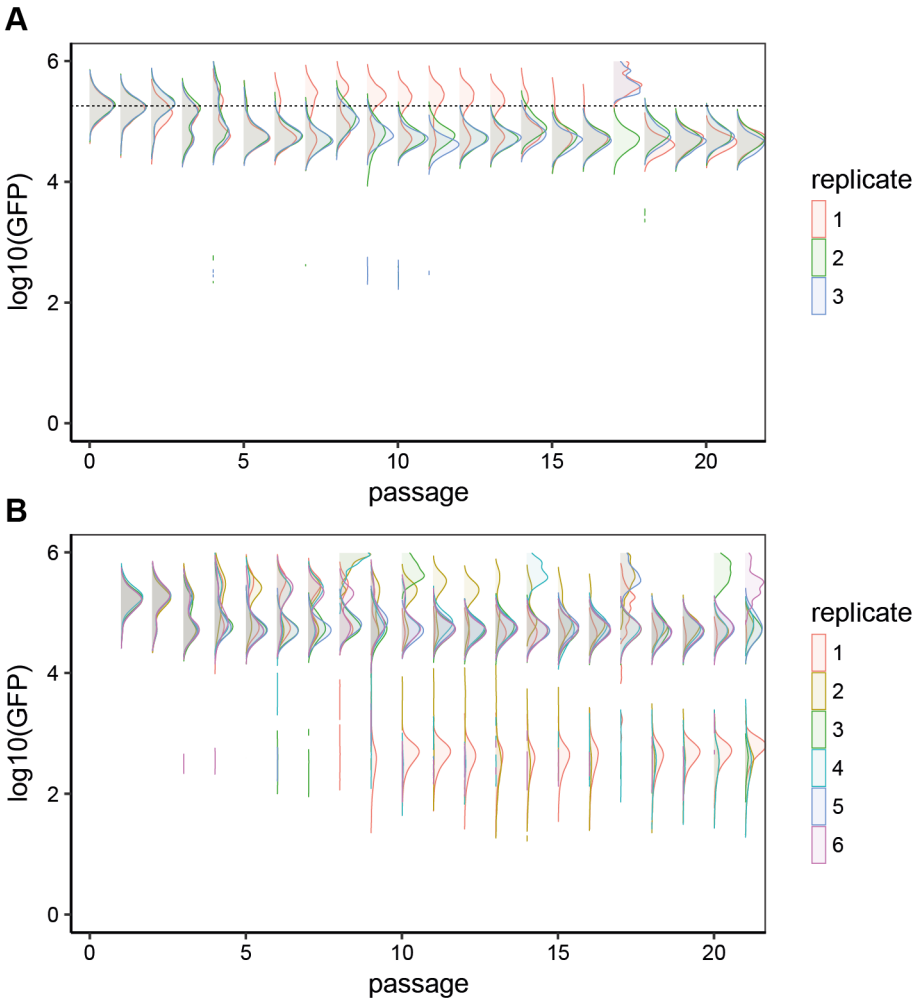

Figure S10: related to Figure 2. Flow cytometry samples of EcN-Lux:ColE1-GFP-HS. A) 3 replicates grown in LB media with erythromycin and kanamycin, ensuring plasmid maintenance. The black dashed line indicates the median fluorescence at passage 0. B) 6 replicates grown in LB media with erythromycin only, allowing for plasmid loss.

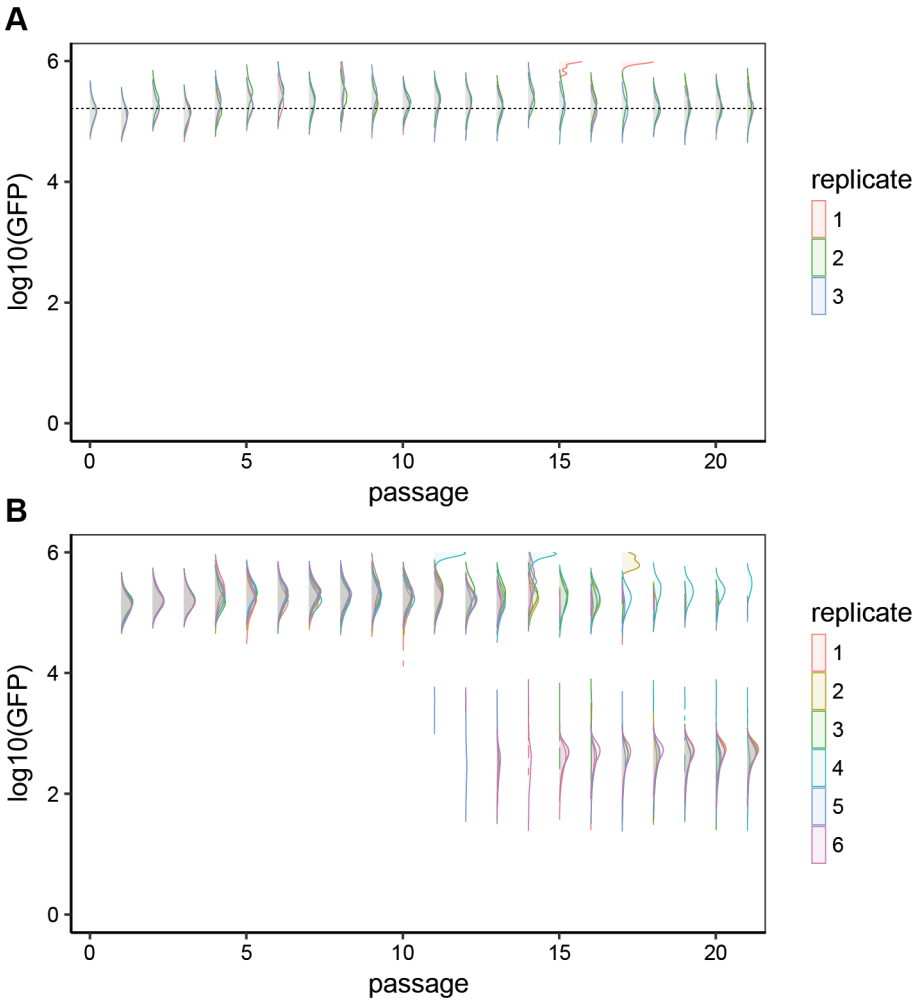

Figure S11: related to Figure 2. Flow cytometry samples of EcN-Lux:pUC-GFP-HS. A) 3 replicates grown in LB media with erythromycin and kanamycin, ensuring plasmid maintenance. The black dashed line indicates the median fluorescence at passage 0. B) 6 replicates grown in LB media with erythromycin only, allowing for plasmid loss.

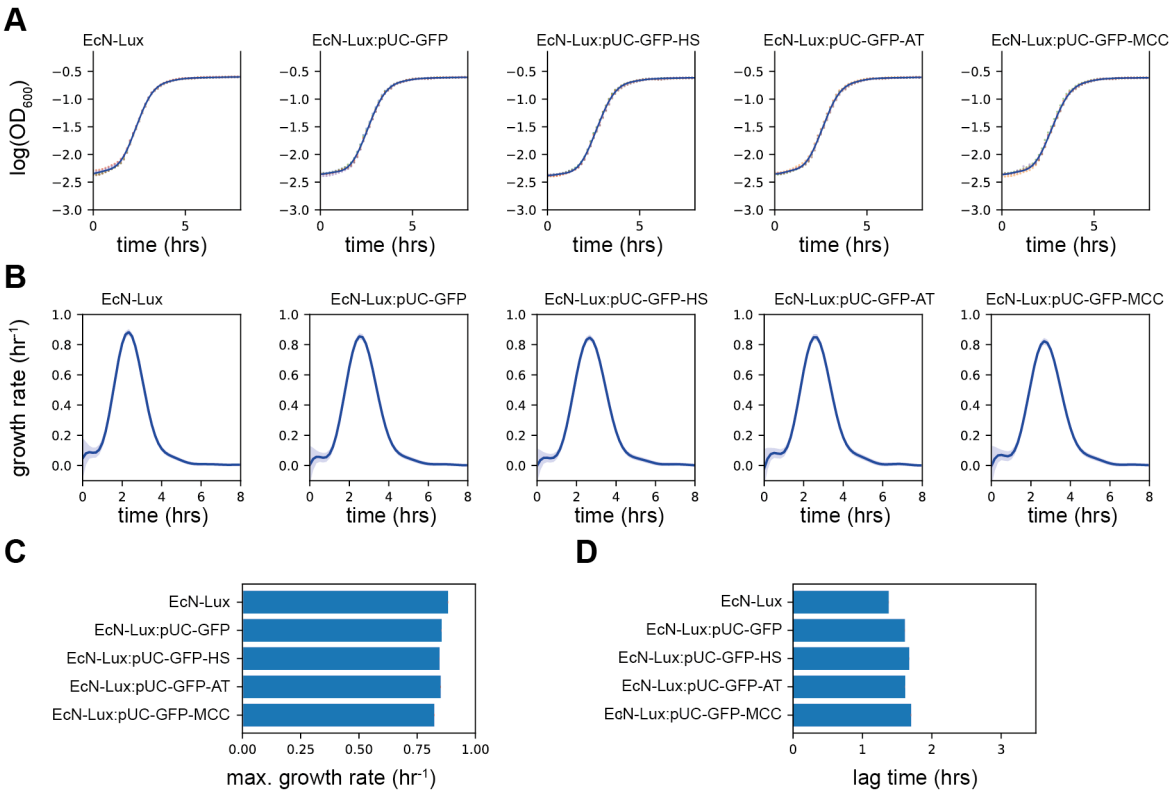

Figure S12: related to Figure 3. Growth curves and model fits for the fluorescent plasmids with different PSK systems in EcN-Lux grown in LB media with erythromycin. (A) Logged optical density measured at 600nm. The points show 6 replicates for each strain with the different colours indicating each replicate. The blue line shows the non-parametric Gaussian process fit with standard error shown by the light blue area around the line. (B) Estimated growth rate as a function of time. (C) Estimated maximal growth rates and (D) estimated lag time. The red lines show the standard deviation of the mean.

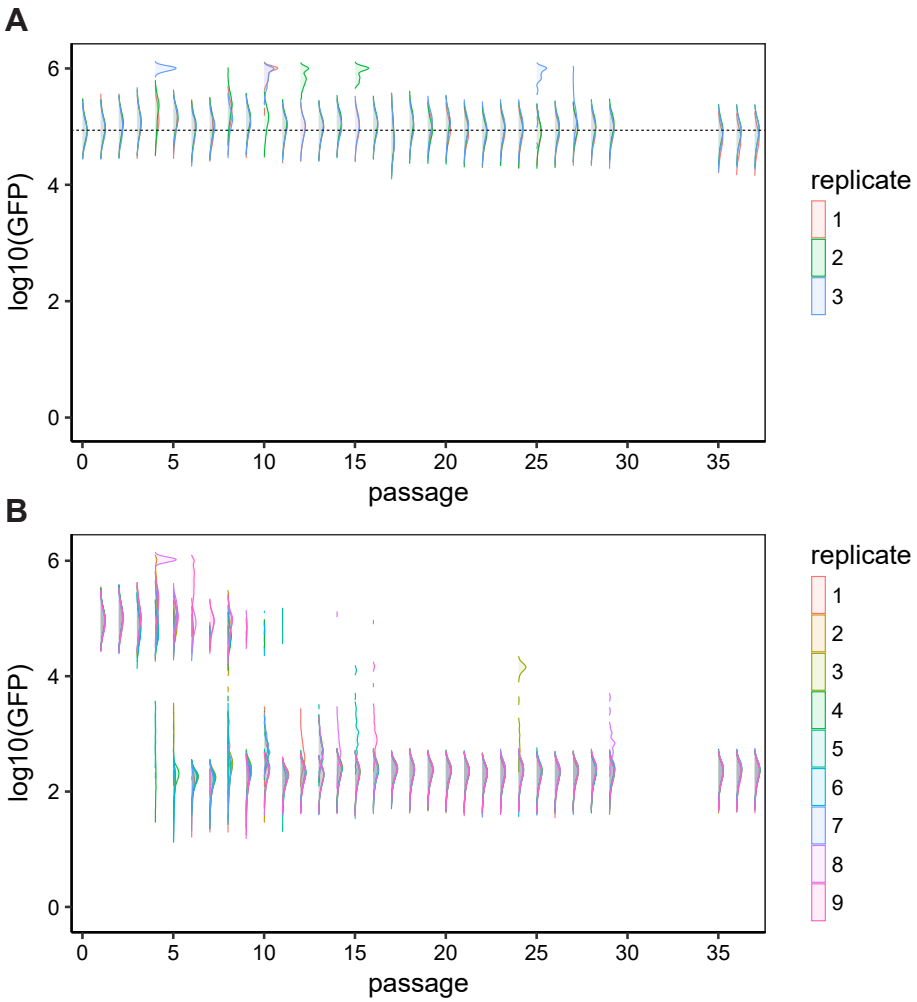

Figure S13: related to Figure 3. Flow cytometry samples of EcN-Lux:pUC-GFP. A) 3 replicates grown in LB media with erythromycin and kanamycin, ensuring plasmid maintenance. The black dashed line indicates the median fluorescence at passage 0. B) 9 replicates grown in LB media with erythromycin only, allowing for plasmid loss.

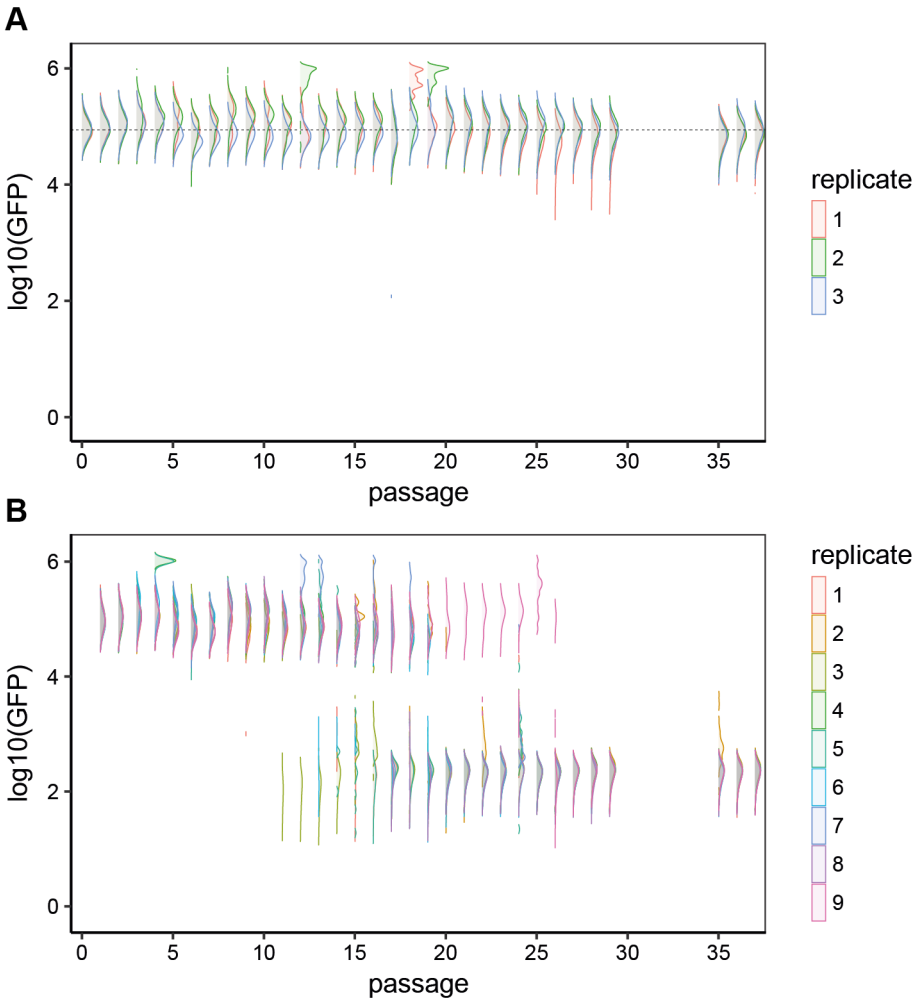

Figure S14: related to Figure 3. Flow cytometry samples of EcN-Lux:pUC-GFP-HS. A) 3 replicates grown in LB media with erythromycin and kanamycin, ensuring plasmid maintenance. The black dashed line indicates the median fluorescence at passage 0. B) 9 replicates grown in LB media with erythromycin only, allowing for plasmid loss.

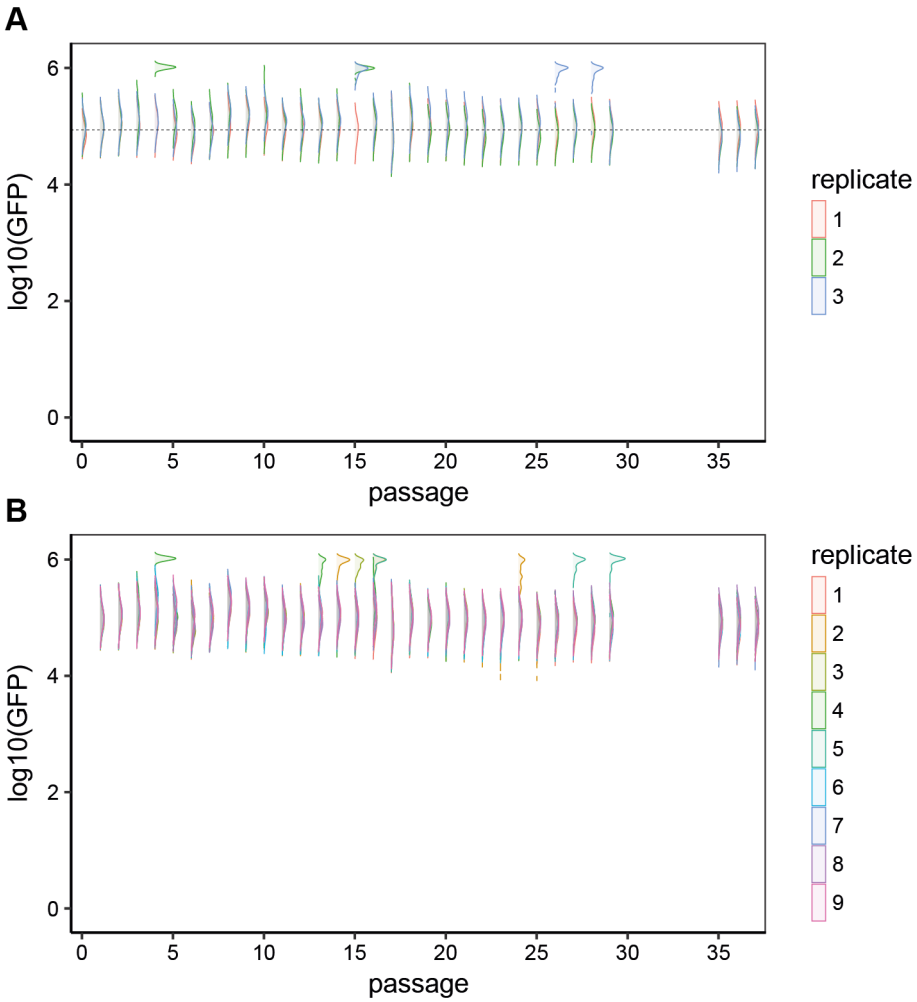

Figure S15: related to Figure 3. Flow cytometry samples of EcN-Lux:pUC-GFP-AT. A) 3 replicates grown in LB media with erythromycin and kanamycin, ensuring plasmid maintenance. The black dashed line indicates the median fluorescence at passage 0. B) 9 replicates grown in LB media with erythromycin only, allowing for plasmid loss.

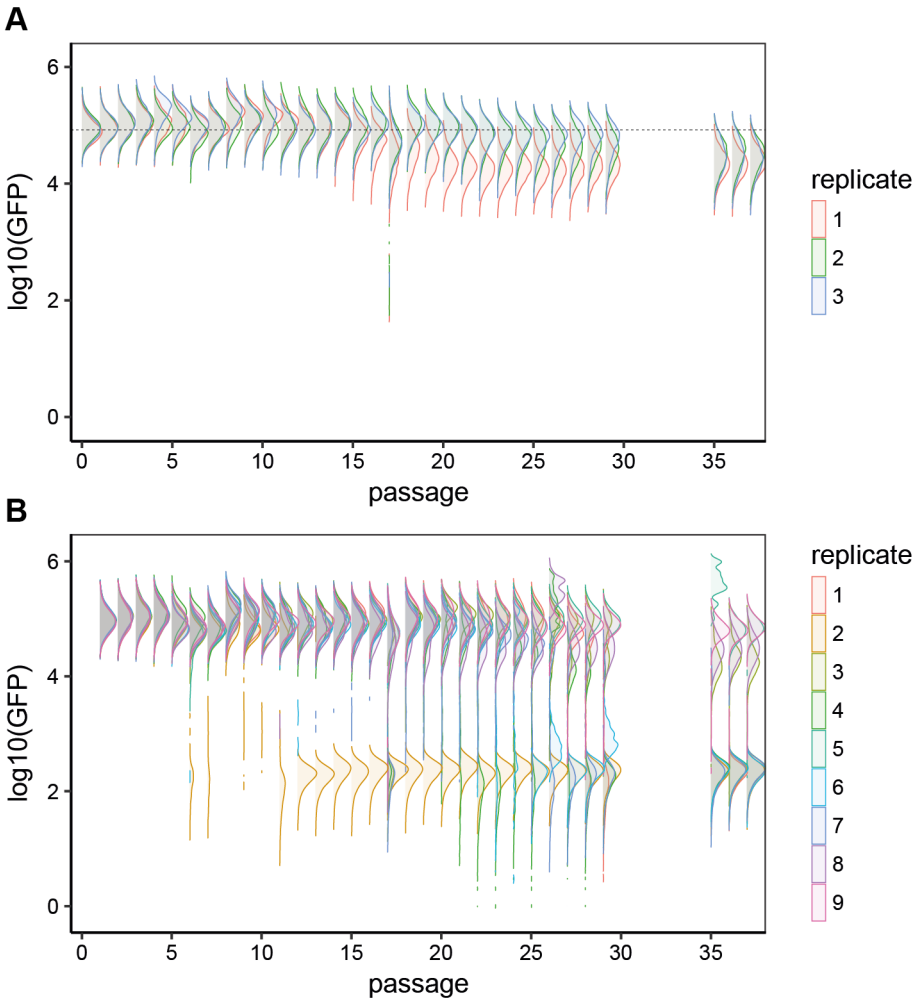

Figure S16: related to Figure 3. Flow cytometry samples of EcN-Lux:pUC-GFP-MCC. A) 3 replicates grown in LB media with erythromycin and kanamycin, ensuring plasmid maintenance. The black dashed line indicates the median fluorescence at passage 0. B) 9 replicates grown in LB media with erythromycin only, allowing for plasmid loss.

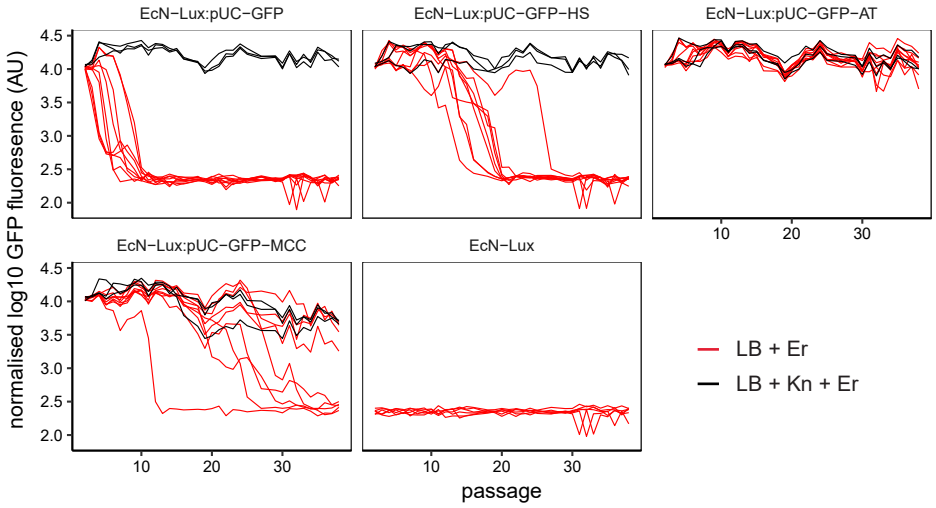

Figure S17: related to Figure 3. GFP fluorescence measurements throughout fluorescent plasmid loss experiment. The black lines (3 replicates) show the trajectories of strains passaged in LB media with erythromycin and kanamycin to ensure plasmid maintenance. The red lines (9 replicates for plasmid-bearing strains and 6 replicates for EcN-Lux control) show the trajectories in LB media with erythromycin but without kanamycin, allowing for plasmid loss. The data is normalised by negating the mean fluorescence of the EcN-Lux in LB+Er (plasmid-free control) at each passage and scaling so that the lowest recorded measurement is equal to 0.

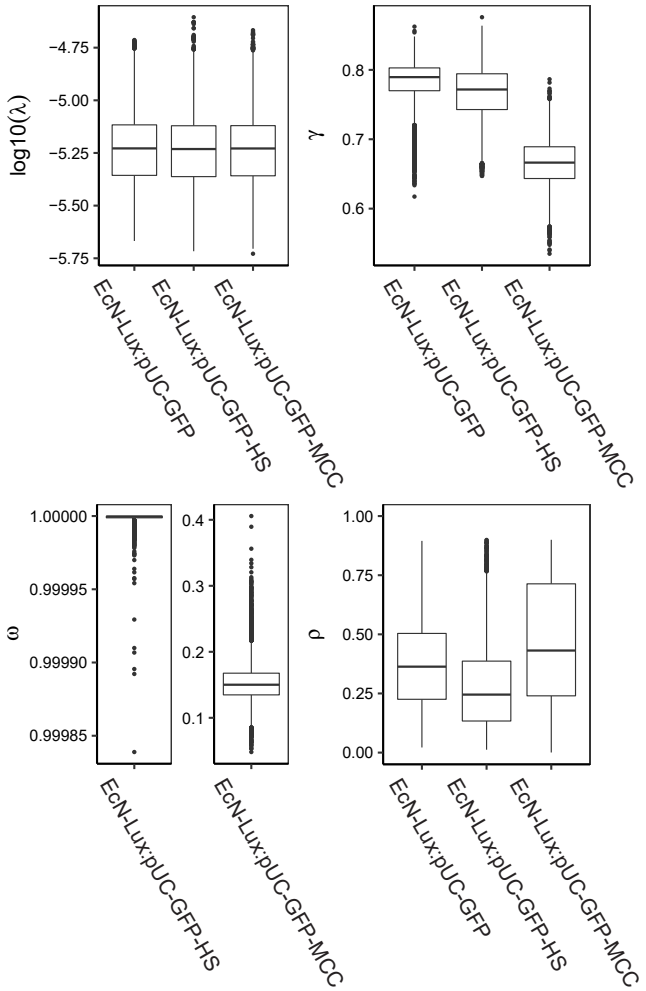

Figure S18: related to Figure 3. Posterior distributions of the model parameters produced from fitting to the plasmid loss curves. EcN-Lux:pUC-GFP has no posterior distribution for ω as it does not carry a PSK system.

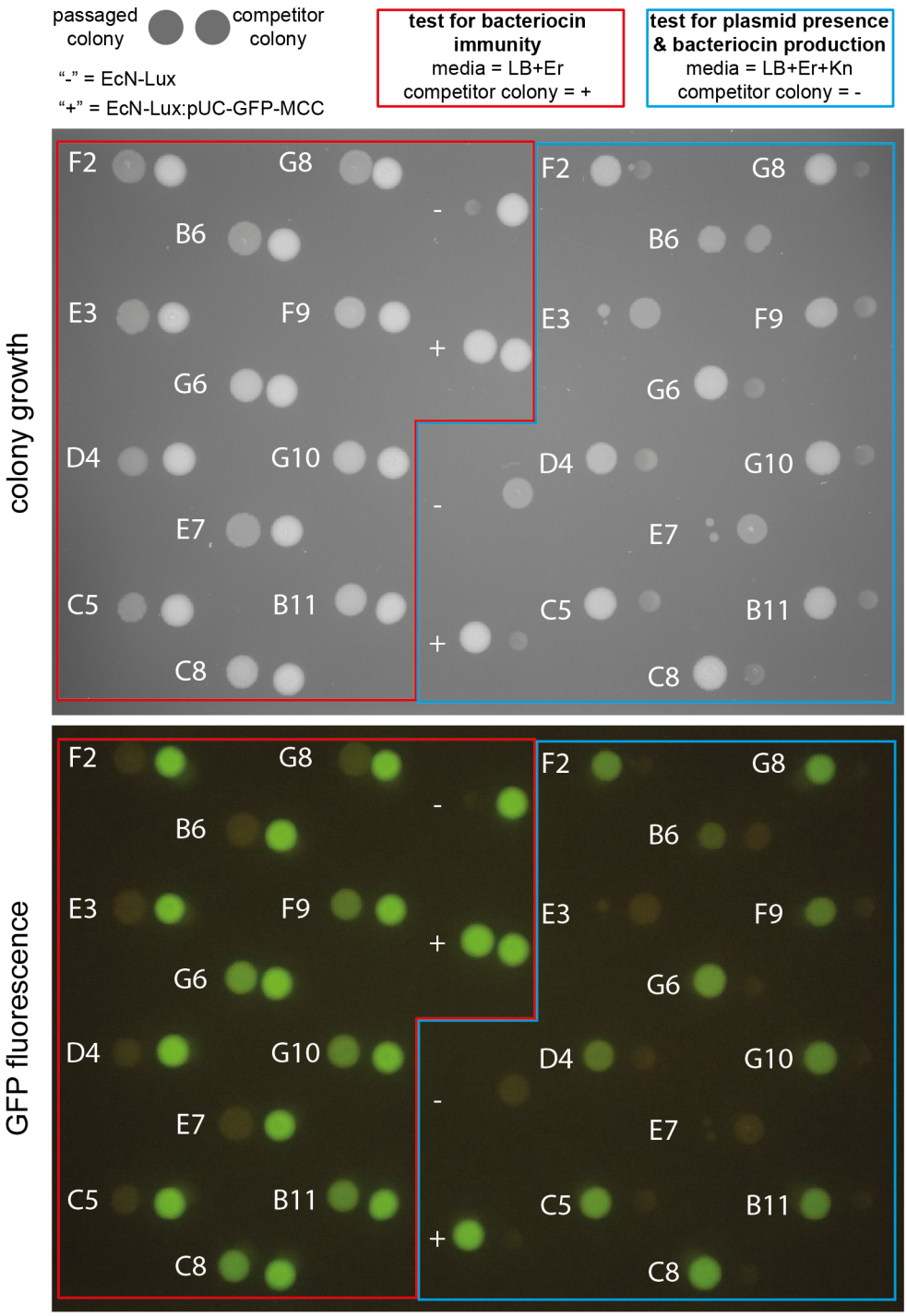

Figure S19: related to Figure 3. Test of bacteriocin production and immunity in EcN-Lux:pUC-GFP-MCC cultures after 30 days of passaged growth. Cultures from the 30th passage of the plasmid loss experiment were grown in LB+Er and LB+Er+Kn and then spotted onto LB+Er agar. The colonies grown in LB+Er were spotted next to a bacteriocin producing colony of EcN-Lux:pUC-GFP-MCC. All of the colonies grow, indicating immunity to the bacteriocin. The negative control, EcN-Lux, shows severely impaired growth. The cultures grown in LB+Er+Kn were spotted next to a bacteriocin sensitive colony, EcN-Lux. Two of the colonies (E3 and E7) show very minimal growth, indicating very limited numbers of plasmid-bearing cells remaining in the source culture. The other colonies show normal growth and increased fluorescence, indicating that the plasmid-bearing cells are still GFP expressing and are being selected for by the kanamycin. All but three of the bacteriocin sensitive colonies show impaired growth. This demonstrates that the plasmid-bearing cells in the source cultures are still producing bacteriocin.

Table S4: related to Figure 3. Summary of results from Figure S19.

Strain	Media	Colony Growth	Competitor Inhibition	Fluorescence
x	LB + Er	Immune to bacteriocin	-	Likely plasmid bearing majority
	LB + Er + Kn	Likely plasmid bearing	Producing bacteriocin	No functional mutation
EcN-Lux:pUC-GFP-MCC passaged in LB + Er	LB + Er	9/9	0/9	3/9
	LB + Er + Kn	7/9	6/9	7/9
EcN-Lux:pUC-GFP-MCC passaged in LB + Er + Kn	LB + Er	3/3	0/3	3/3
	LB + Er + Kn	3/3	3/3	3/3
EcN-Lux -ve control	LB + Er	0/1	0/1	0/1
	LB + Er + Kn	0/1	0/1	0/1
EcN-Lux:pUC-GFP-MCC +ve control	LB + Er	1/1	0/1	1/1
	LB + Er + Kn	1/1	1/1	1/1

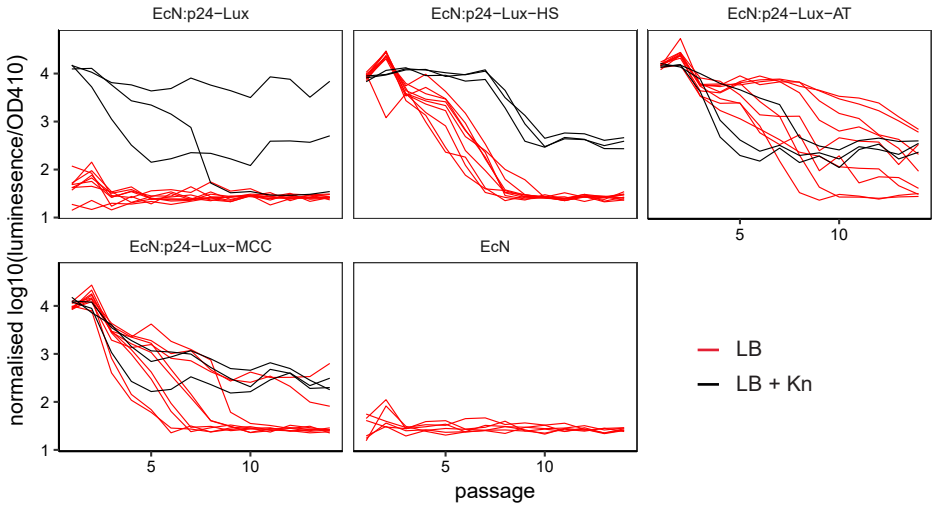

Figure S20: related to Figure 5. Luminescence measurements throughout luminescent plasmid loss experiment. The black lines (3 replicates) show the trajectories of strains passaged in LB media with kanamycin to ensure plasmid maintenance. The red lines (9 replicates for plasmid-bearing strains and 6 replicates for EcN control) show the trajectories in LB media but without kanamycin, allowing for plasmid loss. The data is normalised by negating the mean luminescence of the EcN in LB (plasmid-free control) at each passage and scaling so that the lowest recorded measurement is equal to 0.

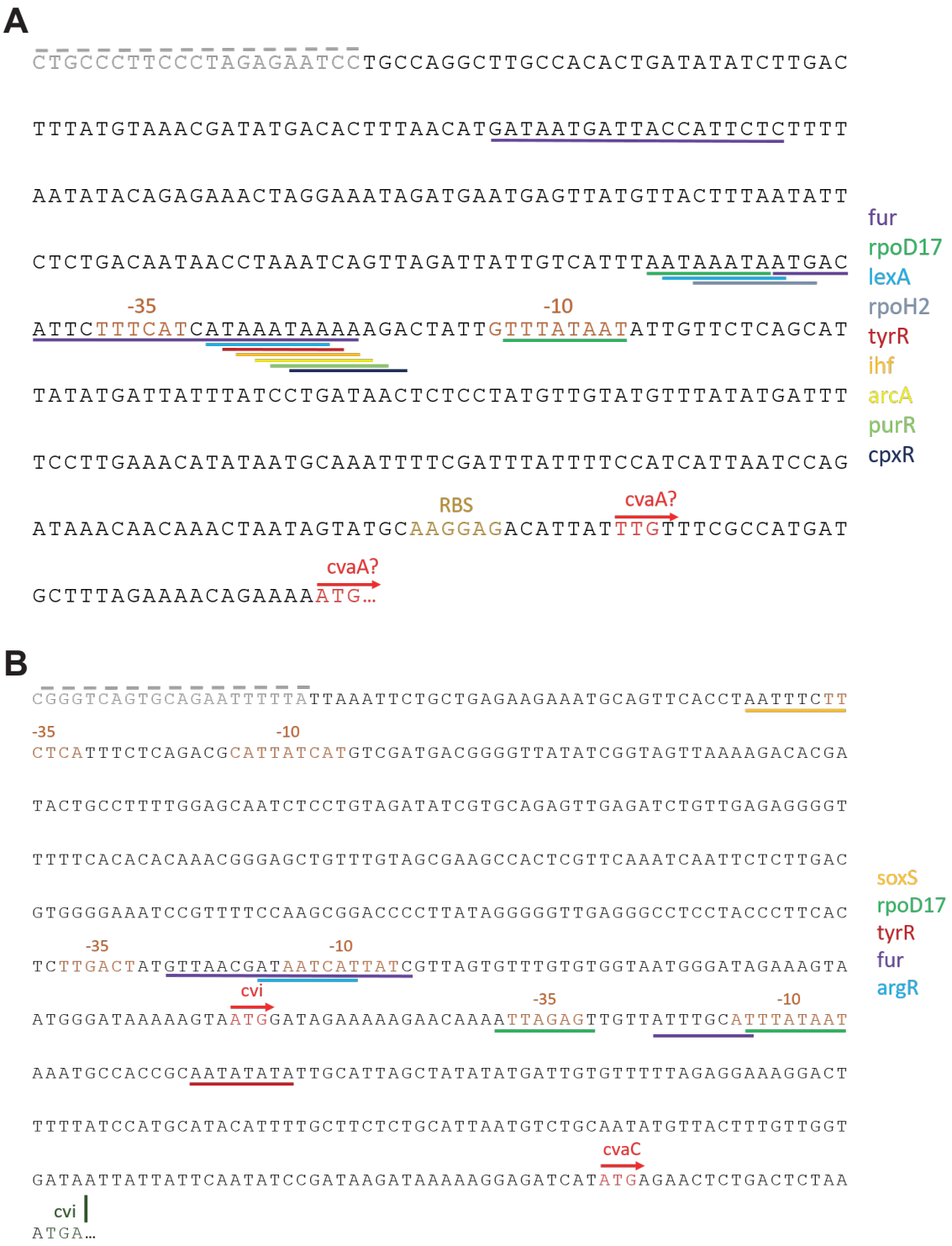

Figure S21: related to Figures 3-5. Upstream regions of microcin-V with -35, -10 and transcription factor recognition sites annotated using BPROM (http://www.softberry.com) A) The region upstream of the cvaA and cvaB genes. Additional annotations of *fur* recognition sites, putative RBS and two potential start codons from Boyer & Tai 1998. B) The region upstream of the cvi and cvaC genes with additional *fur* from Boyer & Tai 1998. Note that there is a putative promoter region after the cvi start codon potentially transcribing the cvaC gene.

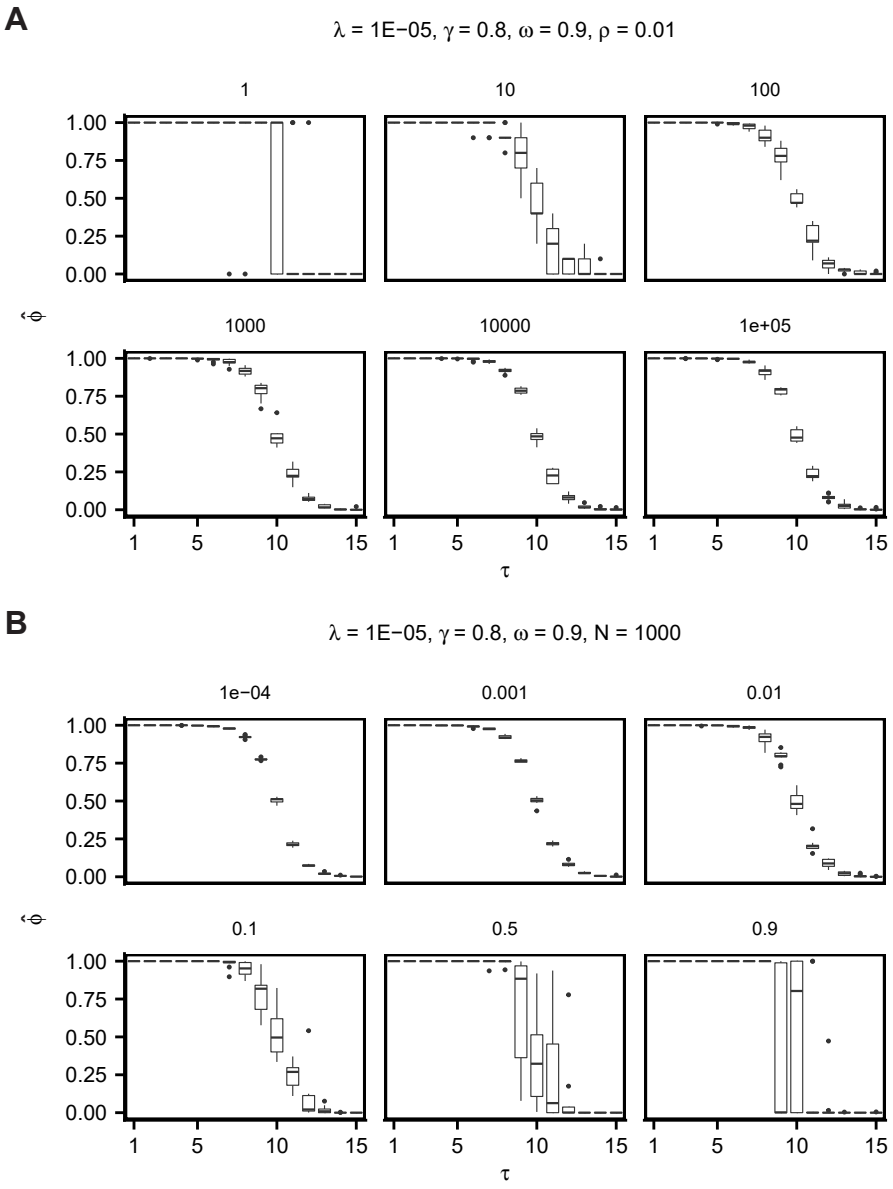

Figure S22: related to Figures 3 and 4. Effects of noise parameters on plasmid-loss curve simulated with the TA model. Nine replicates for each plasmid-loss curve. Varying a) sample size, N, and b) the uncertainty parameter, ρ.

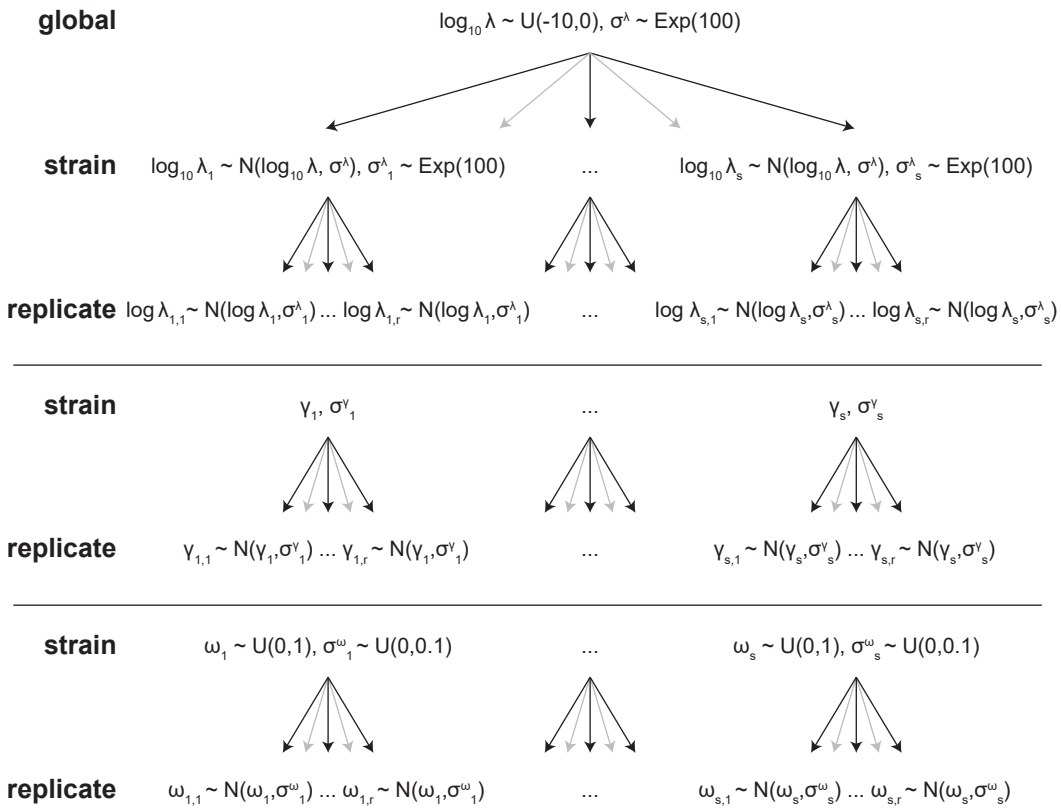

Figure S23: related to Figures 3 and 4. Hierarchical model for fitting parameters of the plasmid loss models to plasmid loss data.

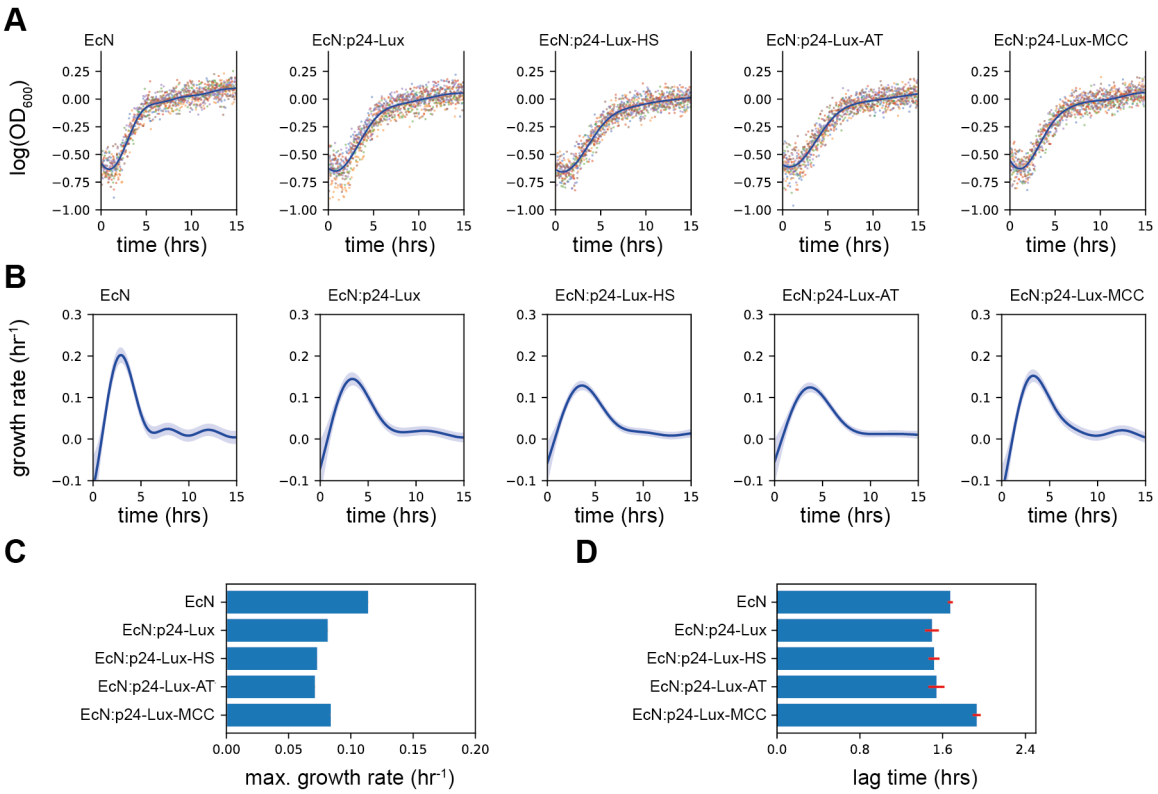

Figure S24: related to Figure 5. Growth curves and model fits for the luminescent plasmids in EcN grown in LB media. For the plasmid bearing strains the media also contained kanamycin to ensure plasmid maintenance. (A) Logged optical density measured at 600nm. The points show 6 replicates for each strain with the different colours indicating each replicate. The blue line shows the non-parametric Gaussian process fit with standard error shown by the light blue area around the line. (B) Estimated growth rate as a function of time. (C) Estimated maximal growth rates and (D) estimated lag time. The red lines show the standard deviation of the mean.

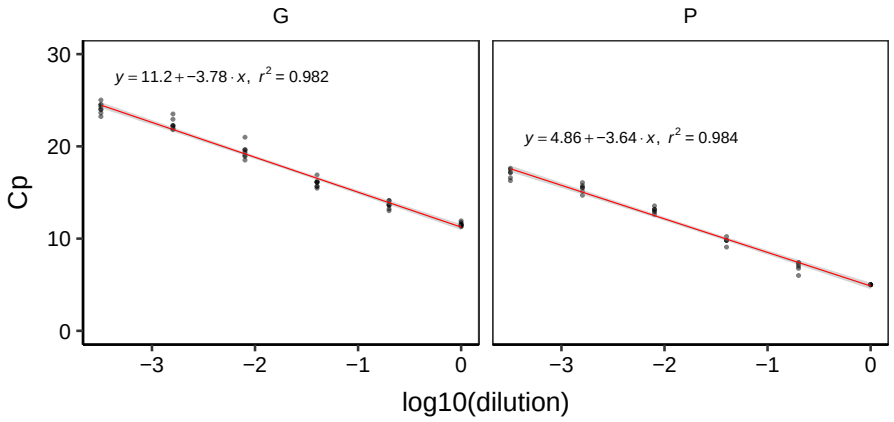

Figure S25: related to Figures 2 and 3. Calibration curves for genomic and plasmid DNA amplification with linear fit (red line).

References

Biernacki, Celeux & Govaert (2000), 'Assessing a mixture model for clustering with the integrated completed likelihood', *IEEE Transactions on Pattern Analysis and Machine Intelligence* **22**(7), 719725.

Carpenter, B., Gelman, A., Hoffman, M., Lee, D., Goodrich, B., Betancourt, M., Brubaker, M. A., Guo, J., Li, P. & Riddell, A. (2016), 'Stan: A probabilistic programming language', *Journal of Statistical Software* **20**, 1–37.

Danino, T., Prindle, A., Kwong, G. a., Skalak, M., Li, H., Allen, K., Hasty, J. & Bhatia, S. N. (2015), 'Programmable probiotics for detection of cancer in urine', *Science Translational Medicine* **7**(289), 289ra84–289ra84.

Gerdes, K. (1988), 'The parB (hok/sok) Locus of Plasmid R1: A General Purpose Plasmid Stabilization System', *Nature Biotechnology* **6**(12), 1402–1405.

Gibson, D. G., Young, L., Chuang, R.-Y., Venter, J. C., Hutchison, C. A. & Smith, H. O. (2009), 'Enzymatic assembly of dna molecules up to several hundred kilobases', *Nature methods* **6**(5), 343–345.

Gilson, Mahanty & Kolter (1987), 'Four plasmid genes are required for colicin v synthesis, export, and immunity.', *Journal of bacteriology* **169**(6), 246670.

Grady, R. & Hayes, F. (2003), 'AxeTxe, a broad-spectrum proteic toxinantitoxin system specified by a multidrug-resistant, clinical isolate of Enterococcus faecium', *Molecular Microbiology* **47**(5), 1419–1432.

Hall, B. G., Acar, H., Nandipati, A. & Barlow, M. (2013), 'Growth rates made easy', *Molecular biology and evolution* **31**(1), 232–238.

Martinez-Garcia, E., Aparicio, T., Goñi-Moreno, A., Fraile, S. & de Lorenzo, V. (2014), 'Seva 2.0: an update of the standard european vector architecture for de-/re-construction of bacterial functionalities', *Nucleic acids research* **43**(D1), D1183–D1189.

Pierce, K. E., Rice, J. E., Sanchez, J. A. & Wangh, L. J. (2002), 'Quantilysetm: reliable dna amplification from single cells', *Biotechniques* **32**(5), 1106–1111.

Riedel, C. U., Casey, P. G., Mulcahy, H., O'Gara, F., Gahan, C. G. M. & Hill, C. (2007), 'Construction of p16slux, a Novel Vector for Improved Bioluminescent Labeling of Gram-Negative Bacteria', *Applied and Environmental Microbiology* **73**(21), 7092–7095.

Sharma, A. (2012), 'An ultraviolet-sterilization protocol for microtitre plates', *Journal of Experimental Microbiology and Immunology (JEMI) Vol* **16**, 144–147.

Silva-Rocha, R., Martinez-Garcia, E., Calles, B., Chavarría, M., Arce-Rodríguez, A., de Las Heras, A., Páez-Espino, A. D., Durante-Rodríguez, G., Kim, J., Nikel, P. I. et al. (2012), 'The standard european vector architecture (seva): a coherent platform for the analysis and deployment of complex prokaryotic phenotypes', *Nucleic acids research* **41**(D1), D666–D675.

Swain, P. S., Stevenson, K., Leary, A., Montano-Gutierrez, L. F., Clark, I. B. N., Vogel, J. & Pilizota, T. (2016), 'Inferring time derivatives including cell growth rates using Gaussian processes', *Nature Communications* **7**, ncomms13766.

Wolfram Research, Inc. (n.d.), 'Mathematica 8.0'.
URL: *https://www.wolfram.com*